 doi: 10.1111/j.1365-246X.2004.02223.x

# Backarc extension and collision: an experimental approach to the tectonics of Asia

Marc Fournier,[1] Laurent Jolivet,[1] Philippe Davy[2] and Jean-Charles Thomas[3]

[1] *CNRS UMR* 7072, *Laboratoire de Tectonique, Université Pierre et Marie Curie, Case* 129, 4 *place Jussieu,* 75252 *Paris Cedex* 05, *France. E-mail: marc.fournier@lgs.jussieu.fr*

[2] *Centre Armoricain d'Etude Structurale des Socles, Université de Rennes* 1, 35042 *Rennes Cedex, France*

[3] *Laboratoire de Géophysique Interne et Tectonophysique, BP* 53, 38041 *Grenoble Cedex* 9, *France*

Accepted 2003 December 13. Received 2003 November 14; in original form 2002 July 26

## SUMMARY

The deformation of the eastern Asian lithosphere during the first part of the India–Asia collision was dominated by subduction-related extension interacting with far effects of the collision. In order to investigate the role of large-scale extension in collision tectonics, we performed analogue experiments of indentation with a model of lithosphere subjected to extension. We used a three-layer rheological model of continental lithosphere resting upon an asthenosphere of low viscosity and strained along its southern boundary by a rigid indenter progressing northward. The lithosphere model was scaled to be gravitationally unstable and to spread under its own weight, so that extension occurred in the whole model. The eastern boundary was free or weakly confined and always allowed eastward spreading of the model. We studied the pattern of deformation for different boundary conditions. The experimental pattern of deformation includes a thickened zone in front of the indenter, a major northeast-trending left-lateral shear zone starting from the northwest corner of the indenter, antithetic north–south right-lateral shear zones more or less developed to the east of the indenter, and a purely extensional domain in the southeastern part of the model. In this domain, graben opening is driven by gravitational spreading, whereas it is driven by gravitational spreading and indentation in the northeastern part where grabens opened along strike-slip faults. The results are compared with the Oligo-Miocene deformation pattern of Asia consecutive to the collision of India. Our experiments bring a physical basis to models which favour distributed deformation within a slowly extruded wide region extending from the Baikal Rift to the Okhotsk Sea and to southeast Asia and Indonesia. In this large domain, the opening of backarc basins (Japan Sea, Okinawa Trough, South China Sea) and continental grabens (North China grabens) have been associated with approximately north–south-trending right-lateral strike-slip faults, which accommodated the northward penetration of India into Eurasia.

**Key words:** collision, continental deformation, experimental tectonics, extension, tectonics of Asia.



## 1 INTRODUCTION

Since Argand (1924) and Molnar & Tapponnier (1975) related the deformation of Asia to the collision of India which started around 50 Ma, numerous analogue and numerical experiments have been performed to characterize the deformation of the Asian continental lithosphere under various conditions of lateral constraint (Tapponnier & Molnar 1976; England & McKenzie 1982; Tapponnier *et al.* 1982; Vilotte *et al.* 1982, 1984, 1986; Houseman & England 1986, 1993, 1996; Davy & Cobbold 1988; Peltzer & Tapponnier 1988; Shemenda & Grokholski 1992; Martinod & Davy 1994; Kong & Bird 1996; England & Molnar 1997; Holt *et al.* 2000; Flesch *et al.* 2001). The debate mainly focused on the geometry of deformation around the collision zone, the degree of localization of the deformation, and the amount of deformation taken up by thickening and lateral extrusion (England *et al.* 1985; England & Houseman 1986; Tapponnier *et al.* 1986; Cobbold & Davy 1988; Dewey *et al.* 1989; England & Molnar 1990; Burchfiel & Royden 1991; Le Pichon *et al.* 1992; Houseman & England 1993; Davy *et al.* 1995). The observations used to argue in favour of one or other of the models were mostly related to the recent and active deformation, i.e. Quaternary fault slip rates (Molnar *et al.* 1987; Avouac & Tapponnier 1993; Peltzer & Saucier 1996; England & Molnar 1997), seismic strain rates (Molnar & Deng 1984; Holt *et al.* 1991, 1995; Holt & Haines 1993; Qin *et al.* 2002) and space geodetic measurements (Molnar & Gipson 1996; Heki 1996;

 

Crétaux *et al.* 1998; Heki *et al.* 1999; Larson *et al.* 1999; Chamot-Rooke & Le Pichon 1999; Holt *et al.* 2000; Shen *et al.* 2000; Flesch *et al.* 2001; Wang *et al.* 2001). However, the deformation pattern of Asia drastically changed around the Middle Miocene because the boundary conditions in eastern and southeastern Asia changed at that time. From the Eocene to the Middle Miocene, extension largely prevailed on the eastern and southeastern margins of Asia where major marginal basins opened above the western Pacific subduction zones. Rather than being stress free, the eastern boundary of Asia was subjected to dynamic extension related to subduction. Several important questions are worth asking about the Oligo-Miocene deformation: (1) How far from the Indian indenter has the Asian lithosphere been deformed? Was the deformation only concentrated around Tibet or was it felt much further as far as the northern Sea of Okhotsk (Kimura & Tamaki 1986; Jolivet *et al.* 1990; Worrall *et al.* 1996)? (2) How much was the opening of marginal basins of eastern Asia shaped by the collision process?

We performed analogue experiments of indentation to understand the role of extension in collision tectonics. Our prime interest was to study the deformation of continental margins subjected to subduction-related extension during indentation. The role of retreating subduction was experimentally simulated by using a gravitationally unstable plate model. In the following, we first present a review of the extensional deformation in Asia since the Eocene to justify the rheology of the models and the boundary conditions of the experiments. We then describe four experiments with different boundary conditions. We discuss the kinematics and geometry of deformation with respect to boundary conditions, paying attention to extensional deformation. We finally compare the deformation of the Asian margins with the experiments.

### 1.1 From extension to compression on the Asian margins: extension in Asia since the Eocene

Far from the collision zone, the Asian lithosphere underwent extension during the Cenozoic (Fig. 1a). From the Eocene to the Middle Miocene, the eastern and southeastern Asian margins were affected by backarc extension. Basins floored with oceanic crust opened: the Celebes Sea in the Eocene (Weissel 1980; Silver *et al.* 1983a; Silver & Rangin 1991a), the South China Sea in the Oligo-Miocene (Taylor & Hayes 1980; Briais *et al.* 1993), the Japan and Okhotsk seas from the Late Oligocene to the Middle Miocene (Tamaki 1988; Tamaki *et al.* 1992; Worrall *et al.* 1996) and the Sulu Sea in the Early Miocene (Silver & Rangin 1991b). Basin systems in Sumatra, the Sunda Shelf, Borneo, the Gulf of Thailand and Malaysia also opened during the Eocene and Oligocene (Hamilton 1979; Daly *et al.* 1991). The opening of marginal basins ceased during the Middle Miocene and resumed in the Okinawa Trough in the Late Miocene (Sibuet *et al.* 1995, 1998). Several models have been proposed to relate backarc extension and spreading to subduction, including secondary induced asthenospheric convection (McKenzie 1969), mass upwelling of the asthenosphere (Karig 1971; Tatsumi *et al.* 1989), gravity or eastward asthenospheric flow acting on a dense subducting slab (Molnar & Atwater 1978; Uyeda & Kanamori 1979) and collapse of a thickened continental margin (Le Pichon 1982; Faccenna *et al.* 1996, 1999).

Extension was not restricted to the Asian margins and also affected the inland part of the continent. Since Eocene time, northern China has experienced distributed extension over the multirifted North China Basin (Fig. 1a; Hellinger *et al.* 1985; Hong *et al.* 1985; Chen & Nabelek 1988; Tian *et al.* 1992; Allen *et al.* 1997) and in the Hetao, Yinchuan and Weihe graben systems surrounding the

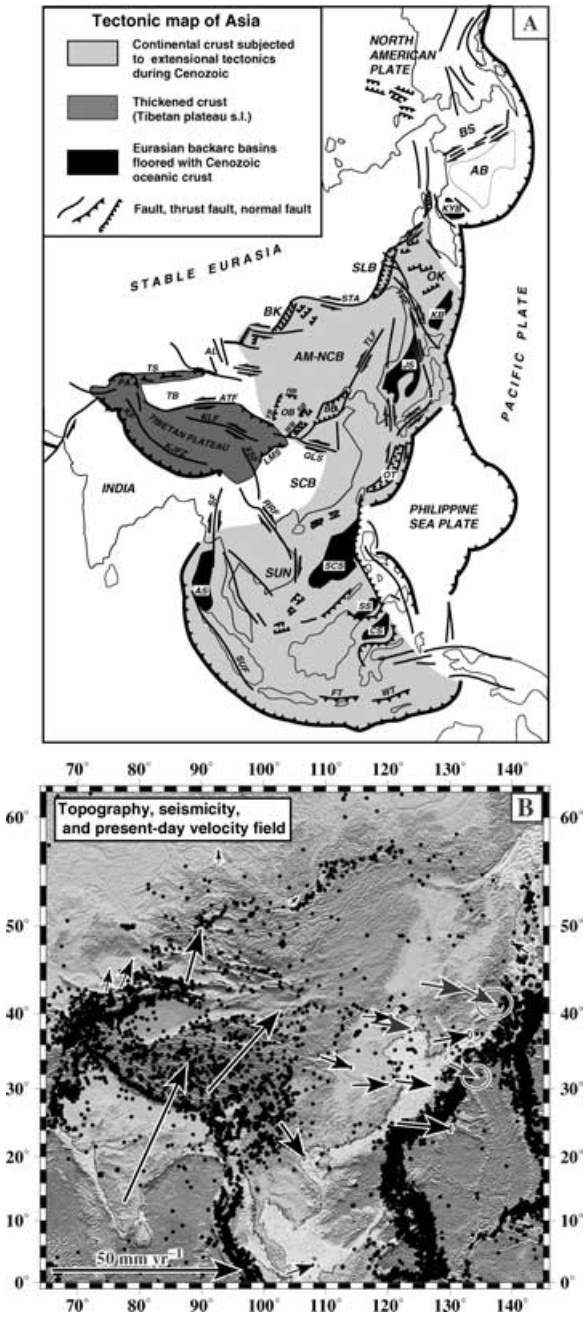


**Figure 1.** Deformation maps of Asia. (a) Tectonic map of Asia: AB, Aleutian Basin; AL, Altai Range; AM, Amur Plate; AS, Andaman Sea; ATF, Altyn Tagh Fault; BB, Bohai Basin; BK, Baikal Rift; BS, Bering Sea; CS, Celebes Sea; FT, Flores Thrust; HB, Hetao Basin; JS, Japan Sea; KB, Kuril Basin; KF, Karakorum Fault; KJFZ, Karakorum–Jiali fault zone; KLF, Kunlun Fault; KYB, Komandorsky Basin; LMS, Longmen Shan; OB, Ordos Block; OK, Okhotsk Sea; OT, Okinawa Trough; PA, Pamir; QLS, Qinling Shan; RRF, Red River Fault; SB, Shanxi Basin; SCB, South China Block; SCS, South China Sea; SF, Sagaing Fault; SLB, Shantar–Liziansky Basin; SS, Sulu Sea; STA, Stanovoy Range; SUF, Sumatra Fault; SUN, Sundaland; TB, Tarim Block; TLF, Tan-Lu Fault; TPF, Tym-Poronaysk Fault; WB, Weihe Basin; WT, Wetar Thrust; XSF, Xanshuihe Fault; YB, Yinshuan Basin. (b) Topographic map of Asia, shallow seismicity (focal depth <50 km; magnitude >2) between 1964 and 1995 (Engdahl *et al.* 1998), and current GPS velocity field (Heflin *et al.*, version 2002.3, http://sideshow.jpl.nasa.gov/mbh/series.html; Heki *et al.* 1999). with respect to the stable Eurasia plate in the NNR (no net rotation) NUVEL-1A plate motion model (DeMets *et al.* 1990; Argus & Gordon 1991; DeMets *et al.* 1994).

Ordos Block (Ma & Wu 1987; Wang 1987; Bellier *et al.* 1988). Extension in the Shanxi graben system, east of the Ordos Block, was initiated during the Pliocene (Xu & Ma 1992). In the Baikal region, extension started during the Oligocene (Tapponnier & Molnar 1979; Hutchinson *et al.* 1992; Deverchère *et al.* 1993), and Windley & Allen (1993) proposed that a mantle plume was responsible for the extension in this area.

Extension also occurred near the collision zone in relation to the growing topography in front of the Indian indenter. It is currently active in the Himalayas and in Tibet (Molnar & Tapponnier 1978; Tapponnier *et al.* 1981; Molnar & Chen 1983; Burg *et al.* 1984; Burchfiel & Royden 1985; Armijo *et al.* 1986, 1989; Burchfiel *et al.* 1992), where it started in the Middle or Late Miocene (Mercier *et al.* 1987; Pan & Kidd 1992; Coleman & Hodges 1995). Bird (1991) proposed a model of extension in Tibet driven by lateral extrusion of the lower crust under the topographic load.

### 1.2 Extension associated with right-lateral strike-slip faulting in eastern Asia

The opening of the main marginal basins and continental grabens of eastern Asia, from the Okhotsk Sea to the South China Sea and to the North China Basin, has been associated with approximately north–south right-lateral strike-slip faulting (e.g. Ren *et al.* 2002).

A right-lateral shear zone running north for over 2000 km from the eastern Japan Sea margin up to northern Sakhalin Island guided the opening of the Japan and Okhotsk seas during the Oligo-Miocene (Fig. 1a; Lallemand & Jolivet 1985; Jolivet & Huchon 1989; Jolivet *et al.* 1991, 1992; Jolivet & Tamaki 1992; Tamaki *et al.* 1992; Fournier *et al.* 1994, 1995). Jolivet *et al.* (1991) estimated the amount of motion along the shear zone at ∼400 km during the opening of the Japan Sea. Jolivet *et al.* (1992) and Fournier *et al.* (1994) showed that the deformation along the shear zone evolved from transtensional near the subduction zone to transpressional in the northern continental part. This led them to relate extension to subduction and strike-slip faulting to continental deformation, i.e. India–Asia collision. Kimura & Tamaki (1986), putting forward the geometry of the deformation in Asia and Jolivet *et al.* (1990), interpreting the laboratory experiments of Davy & Cobbold (1988), had already related the opening of the Japan Sea to the India–Asia collision.

The current opening of the Okinawa Trough is dominated by oblique rifting and north–south dextral shear. The main grabens within the trough are arranged with a dextral *en echelon* pattern and are associated with north–south right-lateral strike-slip faults (Eguchi & Uyeda 1983; Sibuet *et al.* 1987; Imanishi *et al.* 1996; Fournier *et al.* 2001).

Dextral shear has also been recognized along the East Vietnam margin during the opening of the South China Sea in the Oligo-Miocene. Several studies have shown that the Indochina peninsula was strongly deformed at that time between the dextral shear zone which bounds the Indian indenter to the west and the East Vietnam Fault (Marquis *et al.* 1997; Roques *et al.* 1997). Contemporaneous extension south of the Red River Ailao Shan shear zone (Bukhang Dome) and in the Song Hong Basin allowed Jolivet *et al.* (1999) to propose a dextral bookshelf model for the deformation of Indochina during the opening of the South China Sea.

In northern China, Nabelek *et al.* (1987) and Chen & Nabelek (1988) showed that active normal faulting and subsidence in the North China Basin are linked with dextral strike-slip faulting along the East Taihang, Cang Xian-Dongning and Tan-Lu fault systems. They proposed that the North China Basin opened as a pull-apart basin along the right-lateral Tan-Lu fault system (Lu *et al.* 1983; Xu *et al.* 1987), which was confirmed by the structural and stratigraphic study of the Bohai Basin (Allen *et al.* 1997).

### 1.3 Change of boundary conditions in the Middle Miocene

The collisions of the Australian and Philippine Sea plates with the southeastern and eastern Asian margins started in the late Early and Middle Miocene (e.g. Hall 1996, 2002). In Sulawesi, the Sula and Buton blocks, headlands of the Australian Plate, collided first with the north Sulawesi Island Arc, the southeasternmost extension of the Asian margin (Hamilton 1979; Silver *et al.* 1983b; Rangin *et al.* 1990). An intraoceanic subduction was subsequently initiated to the south. At the same time, convergence and shortening started in southeast Asia with the inception of the southeastward subductions of the proto South China Sea and the Sulu Basin in the Palawan and south Sulu Sea trenches respectively (Holloway 1982; Rangin *et al.* 1990). The subduction of the South China Sea, Sulu and Celebes marginal basins in the Manilla, Negros and Cotobato trenches started in the late Middle Miocene (Maleterre 1989). During the Pliocene, the collision zone was duplicated to the south, in Timor, where the northern Australian margin started to collide with the Banda Arc (Audley-Charles 1981; Milsom & Audley-Charles 1986; Charlton *et al.* 1991; Harris 1991). The deformation front progressed northward and, on the northern edge of the Banda Arc, the southward subduction of the Banda Sea Basin was initiated along the Flores and Wetar thrusts (Silver *et al.* 1983b). At the same time, the Borneo and Sunda shelf basins experienced a major inversion, which started during the Miocene around 17 Ma (Daly *et al.* 1991). Sundaland currently behaves as a rigid plate and its motion is controlled by the subduction of the Indian Plate in the Java Trench (Chamot-Rooke & Le Pichon 1999).

Island arcs carried by the Philippine Sea Plate started to collide with the eastern Asian margin in Middle Miocene, first the Bonin Arc in central Japan (Itoh 1988) followed by the Luzon Arc in Taiwan around 5 Ma (Ho 1986). In Japan, the onset of the present-day compressional regime was recorded between 10 Ma and 7 Ma (Jolivet & Tamaki 1992; Tamaki *et al.* 1992). Compression perpendicular to the trenches is documented by dyke and fault set measurements (Nakamura & Uyeda 1980; Yamagishi & Watanabe 1986; Jolivet & Huchon 1989; Jolivet *et al.* 1991), earthquake focal mechanisms (e.g. Yamazaki *et al.* 1985; Fukao & Furumoto 1975) and geodetic measurements (Heki *et al.* 1990; Mazzotti *et al.* 1999, 2001; Henry *et al.* 2001). The later data show a strong coupling between the Japan Arc and the Pacific Plate. Crustal shortening is also taken up by thrust faulting in the northern part of the Philippine Sea Plate (Zenisu Ridge) (Chamot-Rooke & Pichon 1989; Lallemant *et al.* 1989). In Taiwan, collision began during the Pliocene and the present-day convergence rate measured by GPS amounts 86 mm $yr^{-1}$ along N307°E (Yu & Chen 1994). Convergence results in crustal shortening taken up by active thrust faults in the Longitudinal Valley and at the western thrust front.

Collisions of the Australia and Philippine Sea plates with the Asian margins in Middle Miocene time ultimately resulted in the present-day compression generalized to all the boundaries of Asia, except above the Ryukyu Trench where the Okinawa Trough opens. They might have stopped the opening of marginal basins and led to closure. In contrast, landward, northern China has been little affected by the changes of stress regime along the subduction zone and still undergoes strike-slip and normal faulting. Sakhalin has also been preserved from the change of boundary conditions and it is still dominated by strike-slip and reverse faulting, as in Miocene time (Fournier *et al.* 1994; Arefiev *et al.* 2000).

### 1.4 Conclusion

The recent pattern of deformation shows a strong coupling between the Asian (sensu lato) lithosphere and the subducting plates in Japan as well as in Indonesia, whereas before the Middle (southeast Asia) or Late Miocene (Japan) the eastern and southeastern Asian margins were stretched and deformed by extension. The existence of dextral shear zones along the eastern margin of Asia interacting with marginal extension in the Japan Sea region (Lallemand & Jolivet 1985; Jolivet *et al.* 1990, 1994) has been generalized to the whole margin of Asia from the northernmost Okhotsk Sea (Fournier *et al.* 1994; Worrall *et al.* 1996), the North China grabens (Chen & Nabelek 1988), the Ryukyu region (Fournier *et al.* 2001), to the western margin of the South China Sea (Marquis *et al.* 1997; Roques *et al.* 1997). Continental deformation would be responsible through strike-slip faulting for the geometry of opening of the basins, and the component of extension required for the opening would be provided by the subduction.

Tapponnier & Molnar (1976) and Tapponnier *et al.* (1982) first proposed that the south and east Asian boundaries acted as stress-free boundaries during the collision of India and that continental blocks were extruded toward the east. This hypothesis, relying on the asymmetry of the deformation pattern in Asia, is partly corroborated by recent GPS measurements: one-quarter to one-third of the India–Eurasia convergence is currently transferred to the eastward extrusion of continental blocks (Fig. 1b; Molnar & Gipson 1996; Heki *et al.* 1999; Larson *et al.* 1999; Shen *et al.* 2000; Wang *et al.* 2001). Several experiments of analogue and numerical modelling of continental deformation have been performed with passive free boundaries (Tapponnier *et al.* 1982; Vilotte *et al.* 1982; Vilotte *et al.* 1984, 1986; Cohen & Morgan 1986; Davy & Cobbold 1988; Peltzer & Tapponnier 1988; Houseman & England 1993). So far, the influence of dynamic marginal extension upon continental deformation in the context of collision has not been tested by means of models. We performed laboratory experiments of indentation by a rigid indenter of a model of lithosphere subject to gravitational spreading to understand how collision and extension can interact in continental deformation, and how a drastic change of boundary conditions may have an influence on deformation inside the continent.

## 2 THE EXPERIMENTAL PROCESS

Modelling continental deformation requires the choice of suitable boundary conditions and definition of the fundamental behaviour of deforming continental lithosphere. The main difference between analogue experiments and numerical models lies in the response of the lithosphere to stress. In laboratory experiments, the rheological structure of the deformed media generally favours the brittle behaviour (Coulomb's law of friction) by allowing the localization of the deformation in Plasticine (Tapponnier *et al.* 1982; Peltzer & Tapponnier 1988) or in sand layers (Davy & Cobbold 1988; Davy & Cobbold 1991, 1995). On the other hand, numerical models assume that the lithosphere can be described as a continuum, local discontinuities being averaged over a scale of about 50–100 km (Vilotte *et al.* 1982; Vilotte *et al.* 1986; Houseman & England 1986, 1993; Cohen & Morgan 1986). This assumption deserves careful testing since faults exist up to several thousand kilometres. As a consequence, tectonic maps cannot be directly compared with numerical models.

In their experiments, Tapponnier *et al.* (1982) and Peltzer & Tapponnier (1988) imposed a plane strain condition (no thickening) which inevitably resulted in lateral expulsion of rigid blocks sliding past one another along localized zones of deformation. More recent analogue and numerical models (Cohen & Morgan 1986; Houseman & England 1986; Vilotte *et al.* 1986; Davy & Cobbold 1988, 1991; Houseman & England 1993; Houseman & England 1996; Kong & Bird 1996; England & Molnar 1997; Flesch *et al.* 2001) included buoyancy forces, which means that the models thickened in reasonable proportions and thinned when the deviatoric stress exceeded the shear strength. The work of England & Molnar (1997) and Flesch *et al.* (2001) confirms the strong influence of the gravitational potential energy differences on the strain field. Houseman & England (1993, 1996) described numerical experiments with a model including buoyancy forces and with a lithostatic eastern boundary. The deviatoric stress was zero along the boundary, which was allowed to move under the influence of indentation only. Consequently, there was little extension along the eastern margin of the model. Davy & Cobbold (1988) performed analogue experiments with a weakly confined eastern boundary. The deviatoric stress was not zero along the boundary, but the model did not spread because the deviatoric stress was lower than the shear strength of the model. In the first part of this paper, we stated the importance of extensional deformation along the southeastern and eastern boundaries of Asia during the first part of the collision. In continuity with the work of Davy & Cobbold (1988), we attempted to characterize the role of extension during indentation. We built a model of continental lithosphere with a gravity potential higher than its integrated shear strength, so that it could spread under its own weight provided that boundary conditions permitted. With this type of weak unstable lithosphere model, the deformation pattern is more diffuse than for a strong plate. The distribution and the amount of extension in the experiments are therefore not similar to the natural case. Consequently, the experiments cannot be quantitatively compared with the natural examples, but they bring qualitative information about the deformation produced by collision-indentation on an extending plate.

### 2.1 Rheological properties of the model

We used a rheological model of continental lithosphere made of three layers resting upon an asthenosphere of glucose syrup (Davy & Cobbold 1991). The physical parameters for each experiment and the scaling values are given in Tables 1 and 2, respectively. The upper crust is assumed to be brittle with a Mohr–Coulomb frictional behaviour (Byerlee 1968). It is modelled with dry quartz sand, which obeys a frictional sliding Mohr–Coulomb criterion with a negligible cohesion and a frictional angle of $\sim 30^{\circ}$. The lower crust and the upper mantle are modelled with two Newtonian silicone putties of different viscosities and densities, the upper mantle having higher viscosity and density than the lower crust. The silicone putty is a nearly Newtonian fluid which obeys a creep law where deviatoric stress linearly increases with strain rate. The glucose syrup is a Newtonian fluid of low viscosity (10–100 Pa s) and high density ($\sim$1400 kg m$^{-3}$). Further discussion and justification of the experimental method can be found in Davy & Cobbold (1991) and in Faccenna *et al.* (1999).

### 2.2 Boundary conditions

The southern (lower) boundary of the model was strained by a rigid indenter progressing northward (Fig. 2 and Table 1). The northern (upper) and western (lateral left) boundaries of the model were in contact with the rigid experimental box. The eastern (lateral right) and southeastern (lower right) boundaries were 'free', i.e. the lithosphere model was at isostatic equilibrium directly with the

**Table 1.** Physical characteristic of the experiments.

| Exp. number | Thickness (mm) | | | Density ($10^3$ kg m$^{-3}$) | | | Viscosity ($10^4$ Pa s) | | Indenter velocity (cm hr$^{-1}$) | East boundary confinement | $L$ (cm) | Initial spreading, (hr) | Indentation (hr) |
|---|---|---|---|---|---|---|---|---|---|---|---|---|---|
| | BC | DC | DM | BC | DC | DM | DC | DM | | | | | |
| E1 | 5 | 10 | 5 | 1.09 | 1.14 | 1.34 | 4 | 7 | 6.5 | total | 35 | 1 | 3 |
| E2 | 5 | 10 | 5 | 1.09 | 1.14 | 1.34 | 4 | 7 | 5.5 | total | 35 | 0 | 3.5 |
| E3 | 5 | 10 | 5 | 1.09 | 1.19 | 1.28 | 4 | 6 | 7 | no | 24 | 0 | 3 |
| E4 | 8 | 10 | 5 | 1.09 | 1.19 | 1.28 | 4 | 6 | 20 | no | 25 | 0 | 1.5 |

The brittle sand layer is noted BC (brittle crust); the upper silicone layer is DC (ductile crust); the lower silicone layer is DM (ductile mantle). $L$ is the length between the eastern edge of the indenter and the eastern boundary of the model (Fig. 2).

**Table 2.** Scaling of parameters in natural and laboratory systems.

| | Nature | Model (E2) |
|---|---|---|
| Gravitational acceleration, $g$ (m s$^{-2}$) | 9.81 | 9.81 |
| Thickness (m) | | |
| Brittle crust | 10 000 | 0.005 |
| Ductile crust | 20 000 | 0.010 |
| Continental lithosphere, $L$ | 100 000 | 0.020 |
| Scale factor for length: | $L_{\text{model}}/L_{\text{nature}} = 3.3 \times 10^{-7}$ | |
| Density (kg m$^{-3}$) | | |
| Continental lithosphere $\rho_l$ | 3000 | 1200 |
| Asthenosphere $\rho_a$ | 3220 | 1400 |
| Density ratio $\rho_a/\rho_l$ | 1.07 | 1.17 |
| Friction coefficient of brittle layer (m) | 0.5 | 0.5 |
| Viscosity of asthenosphere (Pa s) | $1 \times 10^{20}$ | ~10–100 |
| Velocity of convergence, $u$ (m s$^{-1}$) | $1.3 \times 10^{-9}$ (4 cm yr$^{-1}$) | $1.5 \times 10^{-5}$ (5.5 cm hr$^{-1}$) |
| Characteristic time $t = L/u$ (s) | $7.7 \times 10^{13}$ (2.4 Myr) | $1.3 \times 10^{3}$ (0.37 hr) |

asthenosphere (glucose syrup). In two experiments, the eastern boundary was weakly confined with a 5 mm thick silicone putty layer floating on glucose syrup. This increased the gravity potential of the boundary and slowed down lateral spreading of the model. However, whether it was free or weakly confined, the eastern boundary always allowed lateral spreading of the model.

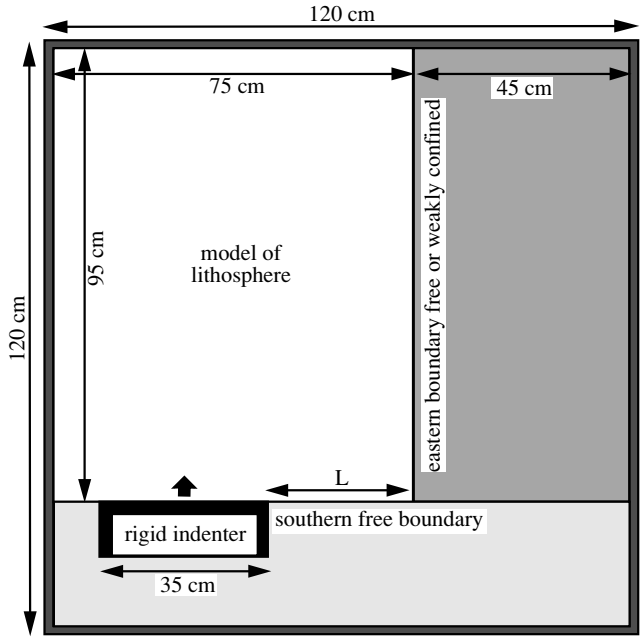


**Figure 2.** Experimental device. The model of continental lithosphere made of three layers (sand, silicone 1, silicone 2) rests upon the asthenosphere made of glucose syrup. It is strained by a rigid indenter which progresses northward.

### 2.3 Scaling for gravitational spreading

The experiments were scaled for the normal gravitational field given the physical properties of materials and setting the thickness of a normal crust, about 30 km in nature, to 1.5 cm in the experiments (Table 2). The initial dimensions of the model are shown in Fig. 2. Under the latter conditions, the width of the model (75 cm) represented 1500 km, its length (95 cm) represented 1900 km, and the width of the indenter (35 cm) represented 700 km which is about one-third of the distance between the two Indian syntaxes. Because of its large dimensions, the model was difficult to build and manipulate and it was not considered possible to build a larger model.

In the experiments, two forces compete in the process of gravitational spreading. The differential hydrostatic pressure between the lithosphere and the asthenosphere favours gravitational collapse of the lithosphere, and the integrated shear strength of the model prevents it. Spreading occurs when the gravity potential of the model with respect to the free boundary exceeds the integrated shear strength of the lithosphere. The ratio between the potential energy difference and the total resistance of the lithosphere corresponds to the Argand number of England & McKenzie (1982) (see also Faccenna *et al.* 1999). The Argand number can be approximated for the experiments in neglecting the shear strength of the silicone putty with respect to that of the sand. The integrated shear strength of the lithosphere becomes a function of the thickness of the sand layer only. The strength of the brittle layer is calculated using the frictional sliding criterion of Ranalli 1995: $\sigma_1 - \sigma_3 = (R-1)\rho g h$, where $R$ is a constant proportional to the coefficient of friction of the sand, which is ~0.5, and $\rho$ and $h$ are the density and thickness respectively of the sand layer. The gravity potential of the model relative to the boundary depends on the thickness of the (brittle and ductile) crust only, as the density of the lithospheric mantle is similar to that of the asthenosphere in the experiments. With these approximations, the Argand number of the experiments is nearly constant and between 3 and 4. These calculations were confirmed by experimental tests, which showed that spreading occurred as soon as the ductile crust was thicker than the brittle crust. We chose a thickness of 0.5 cm for the brittle crust and 1 cm for the ductile crust, i.e. 10 km and 20 km respectively in nature (Tables 1 and 2).

Timescales characteristic of deformations produced by indentation and gravitational spreading have been evaluated. We performed preliminary tests to measure spreading rates in the absence of indentation. The free boundary of a 30 cm large model of lithosphere

advanced at a rate of 1 to 2 cm $hr^{-1}$ (depending on whether the boundary was weakly confined or totally free respectively), which corresponds to a strain rate of (1–2) $\times$ $10^{-5}$ $s^{-1}$ calculated along a line perpendicular to the free boundary. The strain rate produced by indentation calculated along a line perpendicular to the indenter was between $2 \times 10^{-5}$ and $6 \times 10^{-5}$ $s^{-1}$, depending on the speed of the indenter which varied between 6 and 20 cm $hr^{-1}$ (Table 1). Thus, since the timescales characteristic of indentation and gravitational spreading in the experiments were of the same order of magnitude, the two phenomena could interact and be compared with each other.

### 2.4 Testing different boundary conditions

Three parameters were tested during the experiments: the duration of extension, the extension rate and the indentation velocity. The duration of extension and the extension rate control the amount of finite extension.

The duration of extension corresponds to the duration of the experiment. In the first experiment (E1 hereafter), we let the model spread for 1 hr before beginning the indentation. During the initial stage of spreading, homogeneously distributed normal faults appeared in the model. These faults were reactivated during the second part of the experiment under the effect of indentation. In the other experiments (E2, E3 and E4 hereafter), no initial spreading occurred before indentation (Table 1).

The extension rate was controlled by modifying the gravity potential of the model with respect to the eastern boundary, with the presence or the absence of a lateral confinement. The eastern boundary was confined with a 5 mm thick silicone layer in E1 and E2 (Table 1), which increased the gravity potential of the boundary and reduced the spreading rate of the model. In E3 and E4 we removed the confinement and the gravity potential of the model was increased.

The three first experiments were performed with an almost constant indentation velocity between 5.5 and 7 cm $hr^{-1}$ (Table 1). We increased the indenter velocity to 20 cm $hr^{-1}$ for E4.

### 2.5 Method of strain analysis

To record the deformation, the models were covered by an orthogonal grid made of white sand lines spaced every 2 cm. The deformation of the grid was monitored by photography every 15 min. The grids of the initial and final stages were digitized from enlarged photographs. The error margin on the location of the grid nodes is less than 1 mm in the north–south and east–west directions. The finite displacement field with respect to the experimental box is given by the initial and final positions of the grid nodes. A structural map of the final stage of each experiment was drawn from the photographs.

We used continuum mechanics to analyse the deformation. In continuum mechanics, a finite homogeneous strain is described by the deformation gradient tensor ($\boldsymbol{F}$) which gives the relationship between a vector joining two points at the initial and the final stage. $\boldsymbol{F}$ can be decomposed in an antisymmetric matrix which describes a rotation, called the rotation tensor ($\boldsymbol{R}$), and a symmetric matrix which can be related to the strain ellipse (in 2-D) and which corresponds to the usual geological meaning of finite strain, often called a stretch tensor (e.g. Jaeger & Cook 1979; McKenzie & Jackson 1983). Because matrix multiplication is not in general commutative, there are two ways of making this decomposition, depending on whether the rotation is carried out before or after the finite strain:

$$\boldsymbol{F} = \boldsymbol{RU} \text{ or } \boldsymbol{F} = \boldsymbol{VR}$$

where $\boldsymbol{U}$ is the right stretch tensor and $\boldsymbol{V}$ is the left stretch tensor. $\boldsymbol{U}$ and $\boldsymbol{V}$ have the same eigenvalues, which are the principal strains (principal axes of the strain ellipse), but their eigenvectors are different and correspond to the orientation of the principal axes before deformation in the case of $\boldsymbol{U}$, and after deformation in the case of $\boldsymbol{V}$. The finite strain ellipse after deformation, which gives a picture of the local strain, is obtained from $\boldsymbol{V}$ and the surface dilatation, which corresponds to the ratio of the change in area to the original surface, is given by the determinant of $\boldsymbol{U}$, $\boldsymbol{V}$, or $\boldsymbol{F}$. The rotation of the principal strain axes between their initial and final states is calculated from $\boldsymbol{R}$. Finally, we found in the large literature concerned with continuum mechanics a strain tensor known as Almansi–Euler strain tensor ($\boldsymbol{E}$) and defined as:

$$\boldsymbol{E} = 1/2(\mathbf{I} - \boldsymbol{V}^{-2})$$

where $\mathbf{I}$ is the unit matrix (Salençon 1995). The determinant of the Almansi–Euler strain tensor proved to be an excellent indicator of the strike-slip faults in the experiments, that we called 'shear factor' (the determinant of the Almansi–Euler strain tensor is also a good indicator of isotropic contraction, which does not occur in the experiments). It is given between 0 and 1 in non-dimensional units. Thus, a complete set of strain parameters has been obtained to be analysed and compared with the deformation of Asia.

## 3 EXPERIMENTAL RESULTS

### 3.1 Common pattern of deformation

The structural evolution was similar for all the experiments. Experiment 2 (E2) is shown as an example in Fig. 3. Folds and thrust faults first appeared in front of the indenter. After 90 to 120 min of indentation at $\sim$6 cm $hr^{-1}$, a wide left-lateral shear zone trending southwest–northeast was individualized joining the folded zone to the northeast corner of the model. It was associated with antithetic right-lateral shear zones starting from the eastern edge of the indenter, more or less developed depending on boundary conditions (Fig. 3b). In the southeastern part of the model, grabens formed in a large extensional domain exempt from strike-slip fault. Some grabens opened as extrado cracks perpendicular to the curvature of the eastern and southern boundaries. Afterwards, the compression zone in front of the indenter widened. It encompassed a triangular zone preserved from deformation and bounded to the north by *en echelon* folds and thrusts. In the northeastern part of the model, antithetic right-lateral shear zones appeared in the left-lateral deformation zone. They bound rigid blocks which rotated counter-clockwise. Grabens opened at the southern extremities of these right-lateral shear zones (Fig. 3c). At this stage, the deformation pattern was definitively settled. It was asymmetric because the eastern free boundary favoured the development of a major left-lateral deformation zone, which accommodated eastward extrusion.

An analysis of the deformation is shown in Figs 4 to 7 for experiments E1 to E4 respectively, with (a) a structural map at the final stage of the experiment, (b) the finite displacement field relative to the experimental box and (c) a map of the finite strain ellipse. Fig. 8 shows (a) a map of the shear factor, (b) a map of rotation of the principal strain axes, and (c) a map of surface dilatation (changes in surface area) for each experiment.

### 3.2 Diffuse versus localized deformation

The structural maps and the shear factor maps bring complementary information about the degree of localization of the deformation

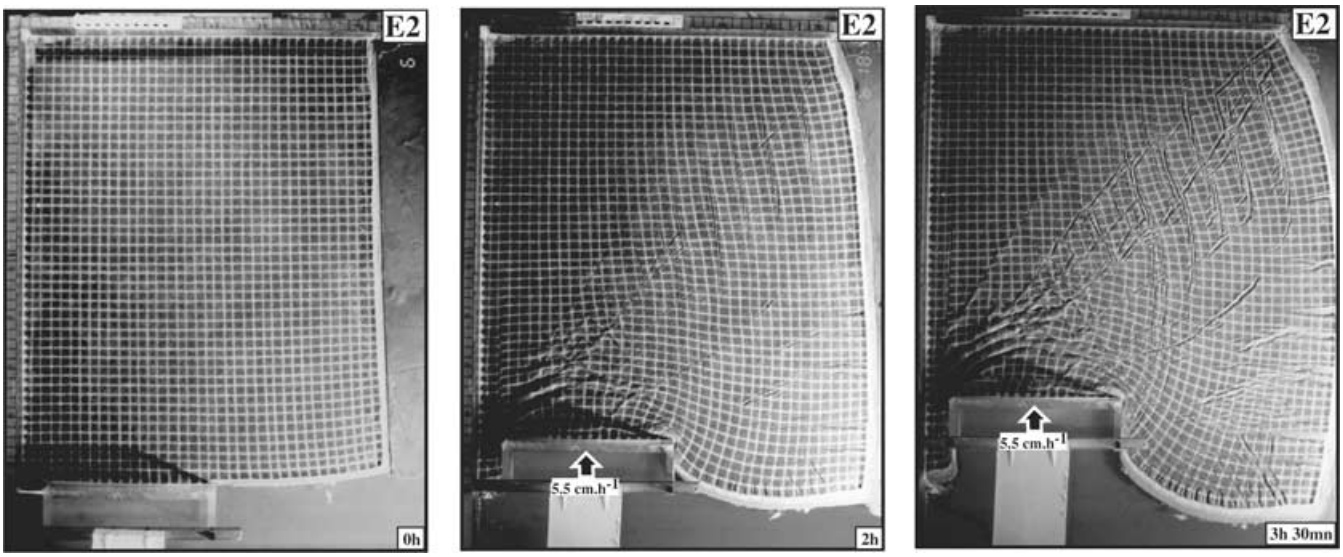


**Figure 3.** Successive deformation stages of E2.

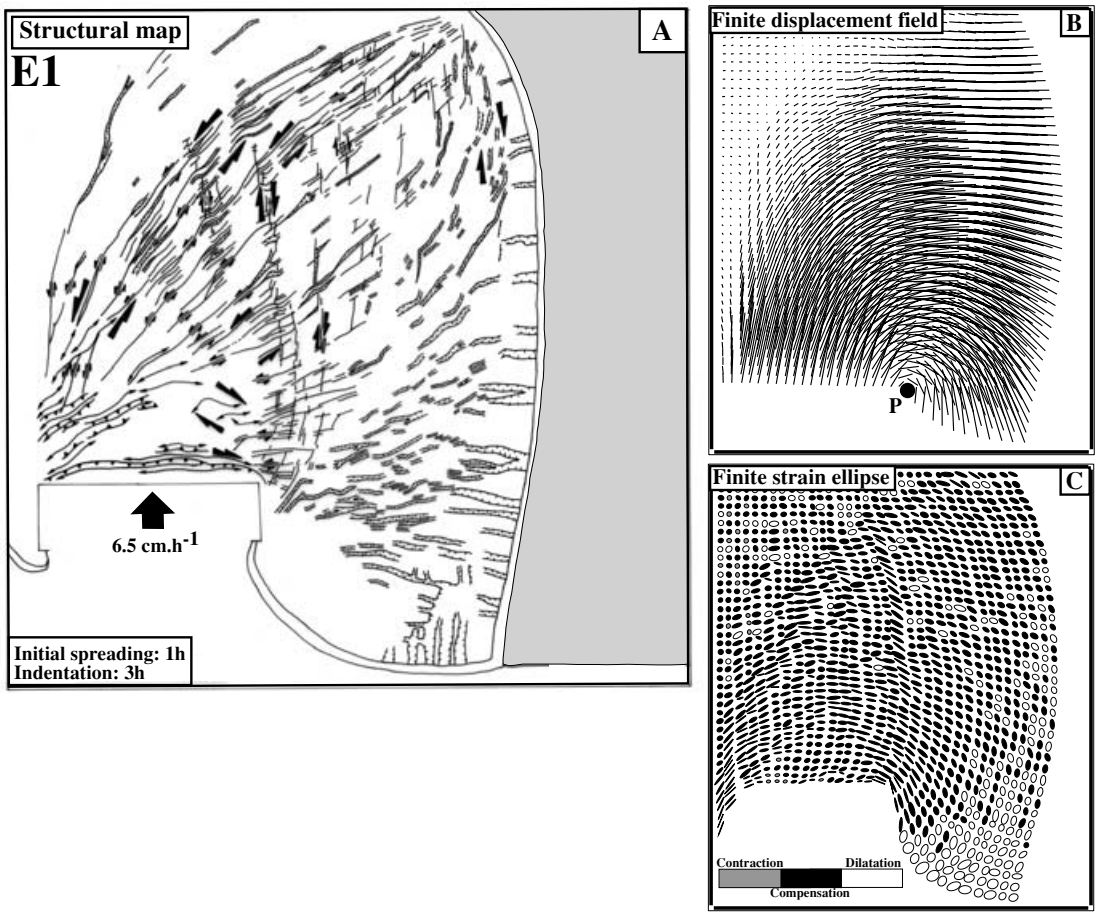


**Figure 4.** Results of experiment E1. (a) Structural map at the final stage of the experiment. Continuous lines are fault traces, which are thrusts (triangle on hangingwall), strike-slip faults, or normal faults (ticks on hangingwall). Folds are continuous lines with arrow at both ends. (b) Finite displacement field relative to the experimental box. (c) Finite strain ellipse.

in the experiments. The shear factor maps show whether the deformation is homogeneous or if it is localized along major faults. The shear factor is maximum near the two edges of the indenter and is always larger on the left side of the indenter, near the fixed wall of the experimental box, than on the right side near the free boundary (Fig. 8a). The shear factor decreases with the distance to the indenter, as the convergence is partly taken up by shortening. In the absence of lateral confinement (E3 and E4) , the deformation

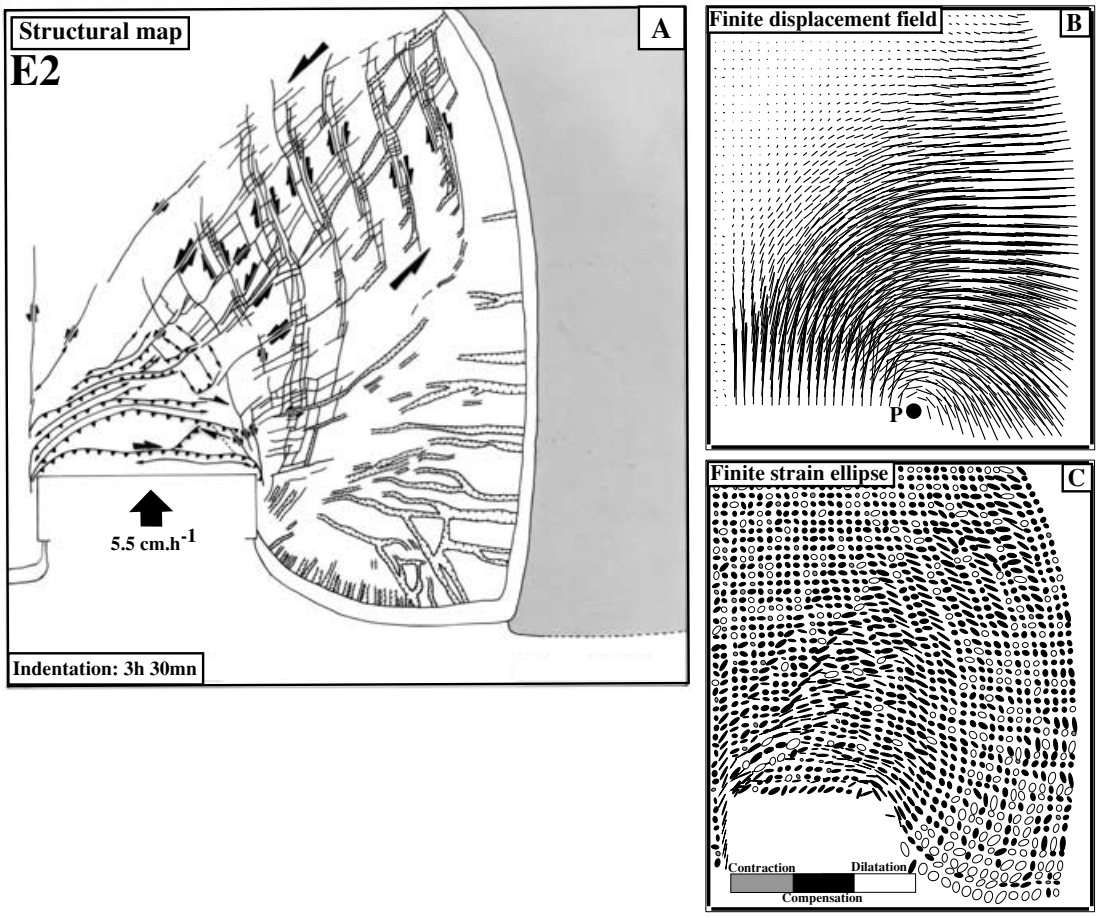


**Figure 5.** Results of experiment E2. Same legend as Fig. 4. The successive stages of E2 are shown in Fig. 3.

is diffuse and accommodated by a dense network of conjugate strike-slip faults (Figs 6a, 7a and 8a). The conjugate faults are distributed almost symmetrically over a triangular deformation zone heading toward the northeast. When the eastern boundary is confined (E1 and E2), the deformation is localized along a few major strike-slip faults (Figs 4a, 5a and 8a). A system of conjugate strike-slip faults appears in front of the indenter. It encompasses a prominent left-lateral shear zone trending southwest–northeast, associated with less developed north–south right-lateral faults starting from the eastern edge of the indenter. Another system of minor conjugate shear zones also appears to the northeast of the unstrained triangle in E1 (Figs 4a and 8a).

In case of preliminary spreading before indentation (E1), the left-lateral strike-slip faults which appear during the indentation partly reactivate normal faults which formed during the preliminary spreading. During the preliminary extension, normal faults were distributed all over the model except in the northwestern corner, with a southwest–northeast mean trend perpendicular to the direction of spreading. The northwesternmost normal faults were curved toward the northwest. In E1, the left-lateral strike-slip faults, which appeared when the indentation began, reactivated these northwestern curved normal faults (Figs 4a and 8a). That is the reason why the deformation pattern in E1 is shifted toward the north in comparison with E2 (Figs 5a and 8a). Thus, in E1 the localization of the deformation occurred after an initial stage of diffuse extension.

### 3.3 Kinematics of finite deformation

Figs 4(b), 5(b), 6(b) and 7(b) show the finite displacement fields relative to the experimental box for each experiment. The displacements are approximately circular about a fixed point (P) with respect to the experimental box, whose position depends on the boundary conditions. The fixed point can be compared with an Euler rotation pole which describes the motion of the main part of the model (except the northwestern corner) with respect to the experimental box, although the deformation is distributed and the model does not behave as a rigid plate. When the eastern boundary is confined (E1 and E2), the fixed point is located immediately east of the indenter (Figs 4b and 5b). The lateral confinement favours extrusion and spreading toward the southern free boundary and the formation of a 'return flow' on the right of the indenter. The mean direction of the 'return flow' changes from approximately north–south in E1 to northwest–southeast in E2, because of the preliminary stage of spreading in E1 which makes a large contribution to the southward component of the 'return flow'. Vilotte *et al.* (1982) obtained a similar displacement field in the case of plane strain with a rigid lateral boundary. In the absence of lateral confinement (E3 and E4), extrusion and spreading toward the eastern boundary are favoured and the fixed point is located further eastward (Figs 6b and 7b). In E3, a substantial 'return flow' appeared to the east of the indenter, whereas in E4 the displacement field is centred on the southeast corner of the model because the high indentation velocity (20 cm $hr^{-1}$) and

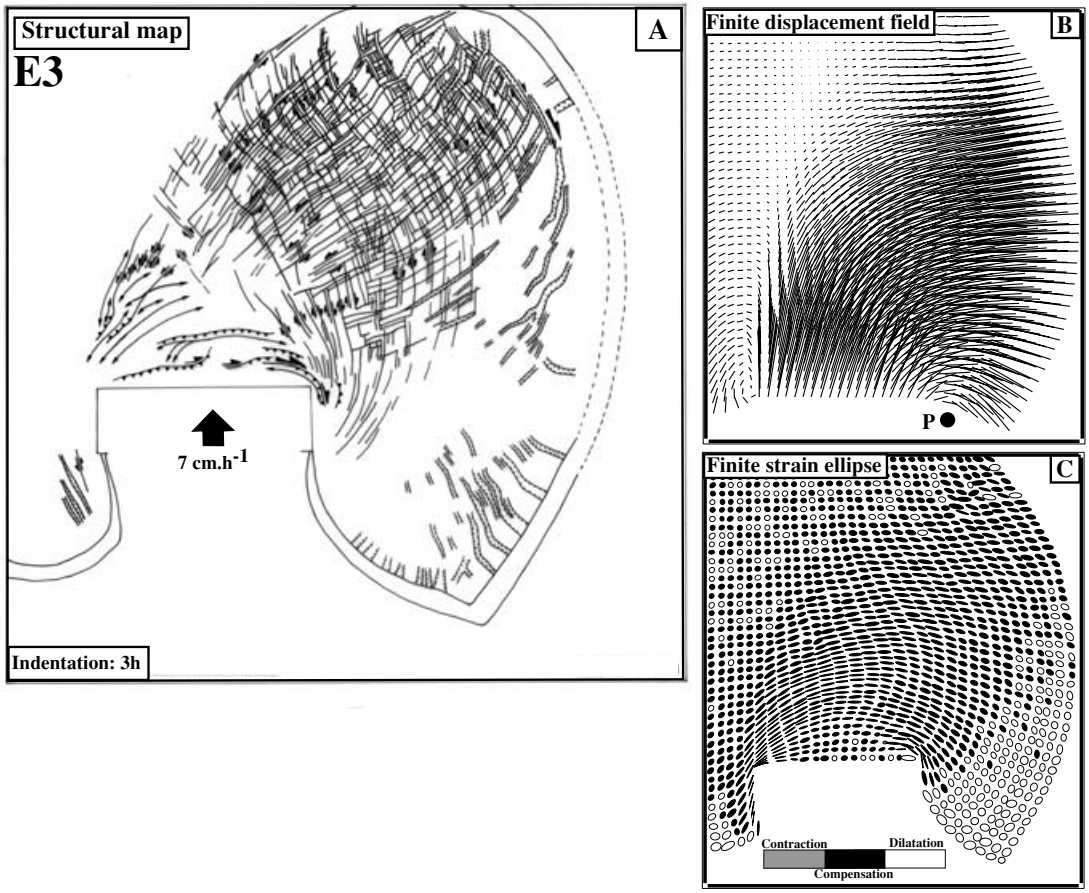


**Figure 6.** Results of experiment E3. Same legend as Fig. 4.

the low duration of the experiment (90 min) prevented southward motion. Similar velocity fields have been obtained in numerical and analogue experiments in the case of plane strain with a free lateral boundary (Vilotte *et al.* 1982; Peltzer & Tapponnier 1988), and the gravitational spreading does not modify this velocity field significantly. Thus, the position of the fixed point mainly depends on the boundary conditions: lateral confinement favours southward escape and brings the fixed point close to the indenter.

The maps of displacement field and shear rate show that the main structure which controls the kinematics of the deformation is the northeast-trending left-lateral shear zone (Figs 4b, 4b, 6b, 7b and 8a). It transforms the northward motion of indentation in eastward extrusion. A component of gravitational spreading toward the free boundaries is added to the component of 'rigid' extrusion (see section 3.4). The north–south right-lateral fault zones, which developed in E1 and E2 from the eastern edge of the indenter, have little influence on the displacement field, though they are well defined on the shear rate maps and accommodated displacements of centimetre scale in the experiments (Figs 4a, 5a and 8a). These displacements are negligible with respect to the eastward displacements. This shows that the choice of faults is of crucial importance in the calculation of displacement field from rates of motion along faults, which already requires a strong hypothesis about the mechanism of deformation.

### 3.4 Rigid extrusion and gravitational spreading

Rigid extrusion can be discriminated from gravitational spreading in the experiments by studying the variations of the eastward component of the velocity along lines originally east–west. Extrusion is defined as the part of the north–south convergence (indentation) which is transferred in lateral motions by the strike-slip faults, the other part being taken up by shortening in front of the indenter. Fig. 9(a) shows the eastward velocity relative to the experimental box versus the distance from the western wall of the experimental box, for each experiment. Velocities have been averaged over a 10 cm wide originally east–west stripe of the central part of the model (i.e. over six east–west lines spaced every 2 cm located between 40 and 50 cm from the southern boundary). The velocity curves in Fig. 9a have a sigmoidal shape and can be divided into three parts corresponding to zones to the west, to the north, and to the east of the indenter. The velocity increases first slowly to the west of the indenter, then quickly to the north of the indenter, and again slowly to the east of the indenter. Fig. 9(b) gives a simple interpretation of these curves. The eastward velocity can be considered as the sum of rigid extrusion and gravitational spreading. In the absence of indentation, the component of gravitational spreading increases linearly from west to east since the silicone putty has a Newtonian behaviour (when the model is thickened by indentation, the gravitational potential of the model increases with the topographic load in front of the indenter, and the spreading velocity increases; however, this effect is negligible in the experimental curves of Fig. 9(a) because the velocities have been measured beyond the thickened zone). During indentation, the eastward velocity increases north of the indenter, as the northward indentation motion is transferred to eastward motion by the left-lateral strike-slip faults. East of the indenter, the eastward velocity increases slowly due to gravitational spreading only. The extrusion velocity can be determined from the experimental curves

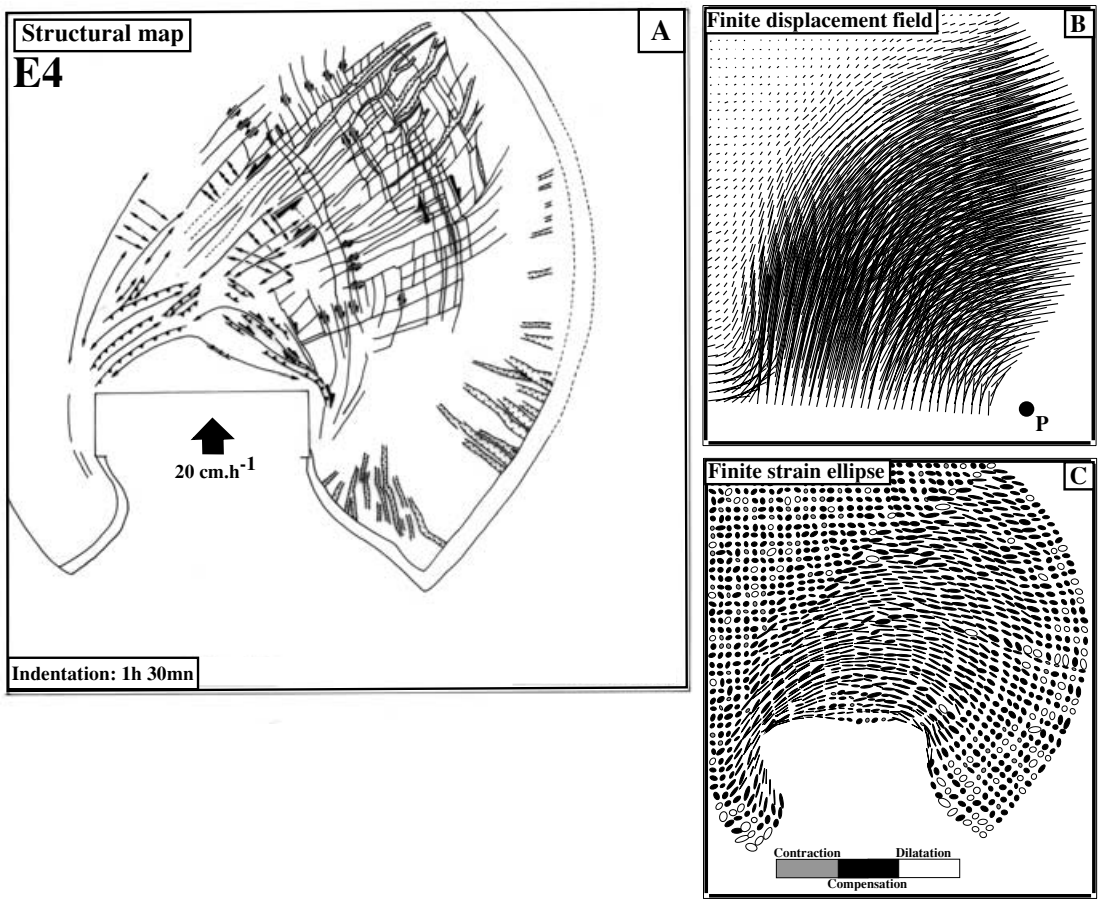


**Figure 7.** Results of experiment E4. Same legend as Fig. 4.

with a linear extrapolation of the gravitational spreading velocity east of the indenter (Fig. 9 and Table 3).

The velocity of gravitational spreading depends on the eastern boundary condition (Table 2): it is between $2.8 \pm 0.8$ and $3.6 \pm 0.6$ cm hr$^{-1}$ when the eastern boundary is free (E3 and E4) and between $0.4 \pm 0.5$ and $0.8 \pm 0.5$ cm hr$^{-1}$ when the boundary is weakly confined (E1 and E2). The extrusion velocity is about one-half of the indentation velocity: it is between $2.5 \pm 0.4$ cm hr$^{-1}$ and $3.6 \pm 0.3$ cm hr$^{-1}$ when the indentation velocity is $\sim$6 cm hr$^{-1}$ (E1, E2 and E3), and it is $11.4 \pm 0.6$ cm hr$^{-1}$ when the indentation velocity is $20 \pm 0.3$ cm hr$^{-1}$ (E4). If the shortening velocity is the indentation velocity minus the extrusion velocity, the shortening/extrusion ratio is about 1 (between 0.8 and 1.8) for the four experiments (Table 3).

### 3.5 Rotations about vertical axes

The rotations are maximum ($>50^\circ$) near the two edges of the indenter where the shear rate is maximum (Fig. 8b). The rotation maps are asymmetric with a prominent northeast-trending stripe of counterclockwise (CCW) rotations corresponding to the major left-lateral deformation zone, and clockwise (CW) rotations in the southeastern part of the model. In the left-lateral shear zone, the CCW rotations reach 20–25° in E1, E2 and E3, and 30° in E4, when the amount of shortening is maximum. In the SE part of the model, the CW rotations exceed 30° in all the experiments. When the deformation is localized (E1 and E2), the stripe of CCW rotations is disrupted by one or several approximately north–south narrow stripes of CW rotations which correspond to conjugate right-lateral shear zones (Fig. 8b). When the deformation is diffuse (E3 and E4), no CW rotation associated with the right-lateral shear zone can be individualized (Fig. 8b).

In the southeastern part of the model, the pattern of CW rotation depends on the boundary conditions. When the eastern boundary is free (E3 and E4), the southeastern part of the model freely rotates clockwise during indentation and the rotation rates increase southward (Fig. 8b). Similar observations were made by Tapponnier *et al.* (1982), Vilotte *et al.* (1984), and Davy & Cobbold (1988) with models with a lateral free boundary. When the eastern boundary is confined (E1 and E2), the model is almost attached to the eastern wall of the experimental box and cannot rotate freely during indentation. The rotations are low along the eastern boundary. The north–south right-lateral shear between the indenter and the eastern boundary is taken up locally on the eastern edge of the indenter. Fig. 3(c) of the final stage of E2 shows that the lines which were originally east–west lines are dextrally sheared on the eastern edge of the indenter and remain approximately east–west near the eastern boundary.

The rotation maps illustrate that rotations can be related either to shear along fault zones or to rotation of large blocks together with faults. They also show that lateral confinement acts upon the deformation of the southeastern part of the model by preventing the free rotation of the model: indentation is accommodated by global

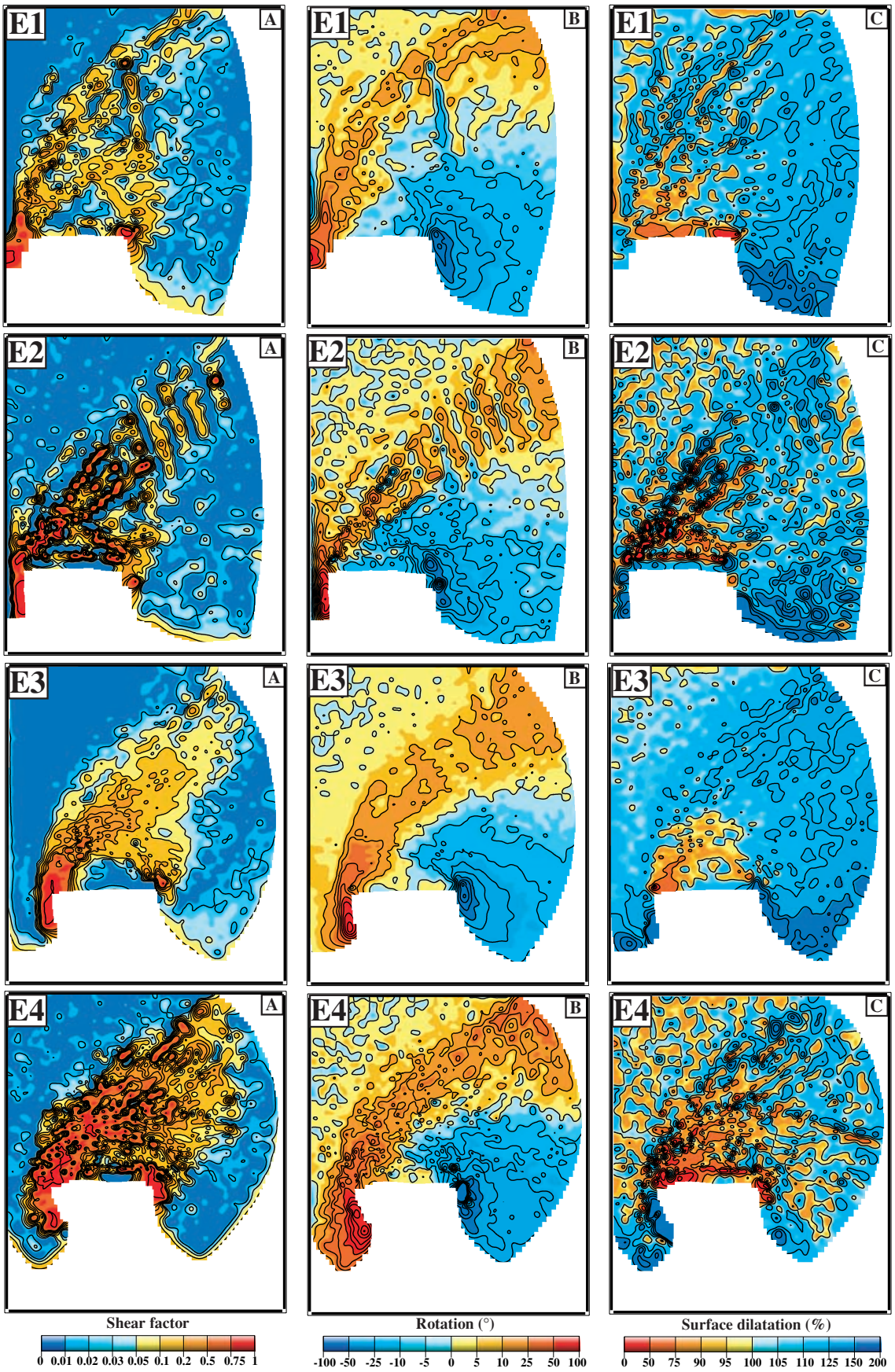


**Figure 8.** Results of experiments E1 to E4: (a) 'shear factor' (determinant of the Almansi–Euler stain tensor, see text), which is an indicator of strike-slip faults; (b) rotation in degree of the principal strain axes; (c) surface dilatation, i.e. ratio of the change in area to the original surface.

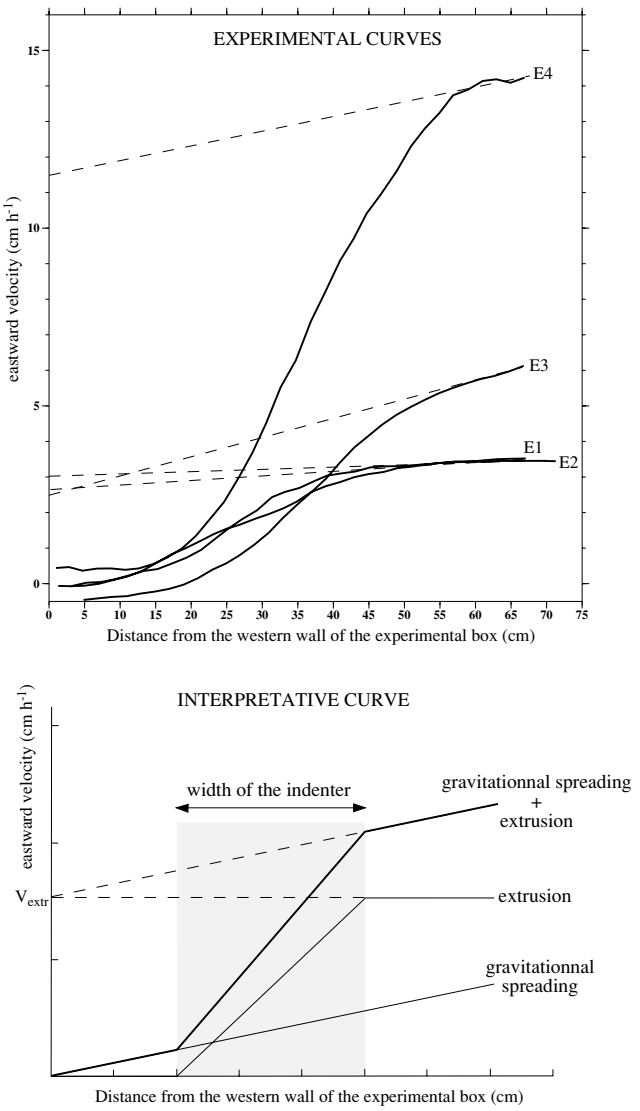


**Figure 9.** (a) Curves of eastward velocity relative to the experimental box versus the distance from the western wall of the experimental box. (b) Interpretation: the eastward velocity is the sum of extrusion and gravitational spreading. $V_{extr}$ is extrusion velocity.

rotation of the southeastern part of the model in the absence of lateral confinement, and by north–south shear to the east of the indenter when the eastern boundary is confined, which isolates the southeastern part of the model from the indentation zone.

### 3.6 Change in area and topography

The surface dilatation (change in area) is expressed as the ratio of the final area of the strain ellipse to its initial area, in per cent (Fig. 8c). The change in surface area corresponds to change in volume during strain, i.e. to change in thickness of the lithosphere model. Hence, they also correspond to variations in topography since the model is at isostatic equilibrium. A decrease in area is equivalent to an elevation of topography, and an increase in area is equivalent to a fall in topography.

Thickening is limited in the experiments because it is quickly compensated by gravitational spreading. Thickening is higher when the indentation velocity is higher (E4; Fig. 8c), or when there is no initial spreading and the eastern boundary is confined (E2; Fig. 8c). The maps show the asymmetric pattern of the thickened lithosphere in front of the indenter. Thickening is more important to the west, near the fixed wall of the experimental box, than to the east near the free boundary. Thickening is localized ahead of the indenter and in the southern part of the northeast-trending left-lateral deformation zone (Fig. 8c). The asymmetric distribution of thickened lithosphere is related to the existence of the left-lateral deformation zone, which localizes part of the thickening.

### 3.7 Driving forces of deformation and opening of marginal basins

The deformation in the experiments is driven by two processes: (1) collision which produces thickening accommodated by folding and thrust faulting, and lateral extrusion accommodated by strike-slip faulting, and (2) gravitational spreading which produces thinning accommodated by normal faulting. Yet it is not easy to discriminate in the finite strain the part related to collision and the part related to gravitational spreading. Following Ramsay (1967), three strain fields have been distinguished on the maps of the finite strain ellipse (Figs 4c, 5c, 6c and 7c). The field of contraction (in grey) corresponds to strain characterized by two shortened principal axes (or quadratic elongation values lower than 1), and the field of dilatation (in white) corresponds to strain characterized by two lengthened principal axes (or quadratic elongation values greater than 1). The intermediate strain field, or field of compensation (in black), is reserved for strain with the least strain axis shortened and the greatest strain axis lengthened.

In the experiments, the northwestern part of the model is equally in the compensation, dilatation or contraction field, because little deformation occurs in this area.

The southeastern part of the model is always in the field of dilatation, which implies that the deformation is driven by gravitational

**Table 3.** Eastward extrusion and gravitational spreading.

| Exp. number | Initial spreading (hr) | Indentation (hr) | Indenter velocity (cm hr$^{-1}$) | Eastward velocity of the eastern boundary (cm hr$^{-1}$) | Velocity of eastward extrusion (cm hr$^{-1}$) | Velocity of eastward gravitational spreading (cm hr$^{-1}$) | Velocity of shortening (cm hr$^{-1}$) | Ratio shortening/ extrusion |
|---|---|---|---|---|---|---|---|---|
| E1 | 1 | 3 | 6.5 | $3.5 \pm 0.2$ | $2.7\ (3.6) \pm 0.3$ | $0.8 \pm 0.5$ | $2.9 \pm 0.6$ | 0.8 |
| E2 | 0 | 3.5 | 5.5 | $3.4 \pm 0.2$ | $3.0 \pm 0.3$ | $0.4 \pm 0.5$ | $2.5 \pm 0.6$ | 0.8 |
| E3 | 0 | 3 | 7 | $6.1 \pm 0.2$ | $2.5 \pm 0.4$ | $3.6 \pm 0.6$ | $4.5 \pm 0.7$ | 1.8 |
| E4 | 0 | 1.5 | 20 | $14.2 \pm 0.2$ | $11.4 \pm 0.6$ | $2.8 \pm 0.8$ | $8.6 \pm 0.9$ | 0.8 |

The eastward velocity of the eastern boundary ($v_b$) and the velocity of eastward extrusion ($v_{ext}$) are obtained from the experimental curves of Fig. 9. For E1, $v_{ext}$ is calculated in parenthesis for the duration of indentation only.
The velocity of eastward gravitational spreading ($v_{sp}$) is: $v_{sp} = v_b - v_{ext}$.
The velocity of shortening ($v_{sh}$) is: $v_{sh} = v_{ind} - v_{ext}$, where $v_{ind}$ is the indenter velocity.
The ratio of shortening/extrusion is: $v_{sh}/v_{ext}$.

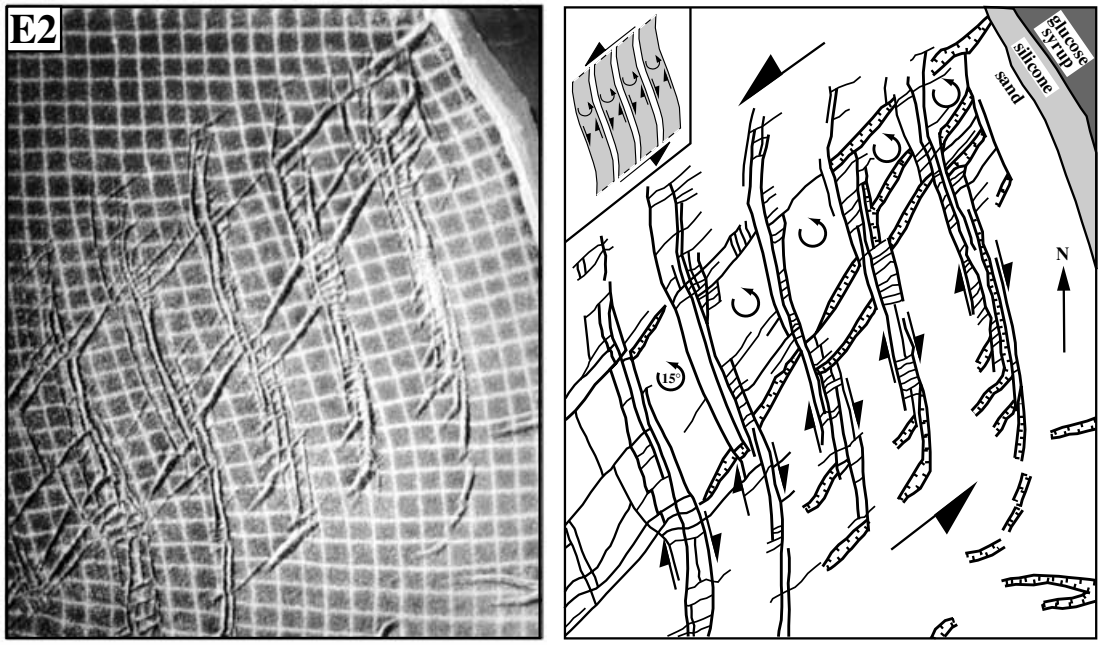


**Figure 10.** Detailed structural map of the northeast part of the model for E3. Grabens form as pull-apart basins between right-lateral strike-slip faults or as tension fractures at the southern extremity of strike-slip faults.

spreading. This part of the model is translated eastward and rotates clockwise under the effect of the indentation, but the influence of indentation upon its internal strain is negligible. The grabens are perpendicular to the direction of spreading: east–west when the eastern boundary is confined and spreading mainly directed toward the south (E1 and E2; Figs 4a and 5a), and northwest–southeast or northeast–southwest when the eastern and southern boundaries are free (flattening prevails) (E3 and E4; Figs 6a and 7a).

The northeastern part of the model is mainly in the compensation field and partly in the dilatation field. It is the place where indentation and gravitational spreading interact and where basins form along strike-slip faults. Fig. 10 show a detailed structural map of this area for E2. Northeast–southwest left-lateral shear in the main deformation zone is accommodated by CCW rotation of rigid blocks bounded by NNW-trending right-lateral strike-slip faults. The blocks rotate 10° to 25° counter-clockwise and the rotation may exceed 10° clockwise in the right-lateral fault zones (Fig. 8b). Grabens form as pull-apart basins between the right-lateral strike-slip faults or as tension fractures at the southern extremity of the strike-slip faults. The geometry of the grabens is entirely controlled by the conjugate strike-slip faults produced by indentation.

### 3.8 Conclusion

The deformation pattern in the experiments is mainly controlled by the gravity potential of the model. The deformation is localized when the gravity potential is limited by confinement of the eastern boundary (E1 and E2), even if indentation has been preceded by preliminary spreading (E1). The deformation is diffuse when the eastern boundary is free and the gravity potential is higher (E3 and E4). The indentation velocity has little influence on the deformation pattern.

The finite displacement field relative to the experimental box is roughly circular about a fixed point located to the east of the indenter. This fixed point moves eastward when lateral confinement is removed. The major structure which controls the kinematics of deformation is the northeast-trending left-lateral deformation zone.

The rotations are related to shear along faults except in the southeastern part of the model which rotates freely in the absence of lateral confinement. When the eastern boundary is confined, the northward motion of the indenter is accommodated by a huge north–south dextral shear zone on the eastern edge of the indenter.

Graben formation is linked with strike-slip faulting related to indentation in the northeastern part of the model, and it is driven by gravity only in the southeastern part.

## 4 COMPARISON WITH THE DEFORMATION OF THE ASIAN LITHOSPHERE

As previously stated, extension is overestimated in the experiments and the results cannot be quantitatively compared with the deformation of Asia. However, they bring qualitative information about the way in which indentation and extension interact and how boundary conditions have an influence upon the deformation far inside the continent.

### 4.1 Current and finite kinematics of Asia

The present-day velocity field in Asia is roughly circular around the eastern Indian syntaxis (Fig. 1b; Molnar & Lyon-Caen 1989; Avouac & Tapponnier 1993; Holt *et al.* 1995, 2000; Peltzer & Saucier 1996; Larson *et al.* 1999), which validates *a posteriori* the hypothesis of Tapponnier & Molnar (1976) of a free boundary along the eastern Asian margin. East of longitude 100°E, southeastern and eastern Asia including Sundaland, South China, North China and the Amurian Plate moves eastward at a mean rate of $\sim$1 cm yr$^{-1}$ relative to stable Eurasia (Molnar & Gipson 1996; Chamot-Rooke & Le Pichon 1999; Heki *et al.* 1999; Larson *et al.* 1999; Shen *et al.* 2000; Wang *et al.* 2001). The relative motions between the main

continental blocks of eastern Asia are low (of the order of few mm $yr^{-1}$), and a wide region extending from the Baikal Rift to the Japan Sea and to southeast Asia and Indonesia is slowly extruded eastward. The present-day velocity field in Asia is thus characterized by an extrusion toward the east, no 'return flow' and a rotation pole to the southeast of the eastern Indian syntaxis. Because of the absence of 'return flow', this velocity field would rather correspond to an experiment with a free boundary to the east, that is E3 or E4.

The finite kinematics of Asia since the Eocene is poorly constrained because it is unclear to what extent extrusion took part in the finite deformation and because the boundary conditions of Asia were different in the Oligo-Miocene. Attempts at reconstruction of the finite displacement field have been realized assuming that Asia is a mosaic of rigid crustal blocks bounded by faults (Cobbold & Davy 1988; Replumaz 1999). These reconstructions rely mainly on the extrapolation over large periods of the current velocity field and Quaternary fault slip rates, and the error margins remain important. Nevertheless, the directions of relative motion in southeast Asia are fairly well constrained for the Oligo-Miocene period. The strike-slip motions along the Red River Fault and the eastern coast of South Vietnam can be described with a rotation pole located east of the Indian indenter (8°N, 86°E; Leloup *et al.* 1995, 2001; Harrison *et al.* 1996; Marquis *et al.* 1997; Roques *et al.* 1997), which also corresponds to the opening pole of the South China Sea (Briais *et al.* 1993). This pole, which accounts for the main relative motions in southeast Asia during the 32–17 Ma period, is near the eastern Indian syntaxis. If this Euler pole could be assimilated to the fixed point of the experiments, it would rather correspond to an experiment with a confined boundary to the east, that is E1 and E2.

Palaeomagnetism provides a complementary approach to the finite kinematics of Asia, independent from fault patterns and slip rates. Palaeomagnetic studies of Cretaceous formations allowed the proposal of reconstructions of Central Asia prior to the collision of India, in which the total amount of north–south convergence between India and Asia is distributed within the Asian Plate (Chen *et al.* 1993; Halim *et al.* 1998). Halim *et al.* (1998) showed that the convergence between the northern Asian blocks and stable Siberia was too large to have been taken up by shortening only in the Tien Shan and Altay mountain ranges. They concluded that the Pamir–Okhotsk deformation zone played a major role during the collision and accommodated several hundred kilometres of left-lateral strike-slip motions between deforming Asia and the Siberian Platform. Evidence for left-lateral motions has been described along this deformation zone. From Tien Shan to Altai, the *en echelon* arrangement of the mountain ranges suggests left-lateral shear (Argand 1922; Cobbold & Davy 1988; Thomas *et al.* 2002). In the Baikal region, normal slip prevails on northeast-trending fault planes, associated with left-lateral slip along east–west strike-slip faults (Tapponnier & Molnar 1979; Hutchinson *et al.* 1992; Deverchère *et al.* 1993). In the Stanovoy ranges, left-lateral slip is evidenced along active east–west strike-slip faults by earthquake focal mechanisms (Parfenoy *et al.* 1987). Worrall *et al.* (1996) showed that the left-lateral deformation extended to the northernmost part of the Sea of Okhotsk and the Bering Strait through a series of northeast–southwest-trending grabens associated with east–west left-lateral faults zones. This major left-lateral deformation zone, which cut Asia from Pamir to the Okhotsk Sea, is still currently active (Fig. 1b). It is equivalent to the northeast-trending left-lateral deformation zone which appears in all the laboratory experiments when the eastern boundary is free.

### 4.2 Rotations in southeast Asia

Clockwise rotations have been widely documented by palaeomagnetism in Cretaceous formations of southeast Asia (Achache *et al.* 1983; Otofuji *et al.* 1990; Funahara *et al.* 1992, 1993; Huang & Opdyke 1993; Chen *et al.* 1993; Halim *et al.* 1998). It has been demonstrated that some of these rotations occurred during the Palaeocene (Funahara *et al.* 1992). Palaeomagnetic data do not show that southeast Asia rotated as a single coherent unit in response to the India–Asia collision, but suggest that most of the rotations occurred before the onset of the collisions of the Australian and Philippine Sea plates with the Asian margins in Middle Miocene time. This situation can be compared with the experiments E3 and E4 with an eastern free boundary. When the model is not attached to the experimental box, the southeastern part of the model rotated freely during indentation (Fig. 11a).

On the other hand, Cobbold & Davy (1988) and England & Molnar (1990) pointed out that the present-day deformation of the eastern margin of Tibet is dominated by large left-lateral active strike-slip faults which separate blocks that are rotating clockwise in a huge north–south right-lateral shear zone (Dewey *et al.* 1988; Huang *et al.* 1992). This shear zone allows the northward motion of Tibet

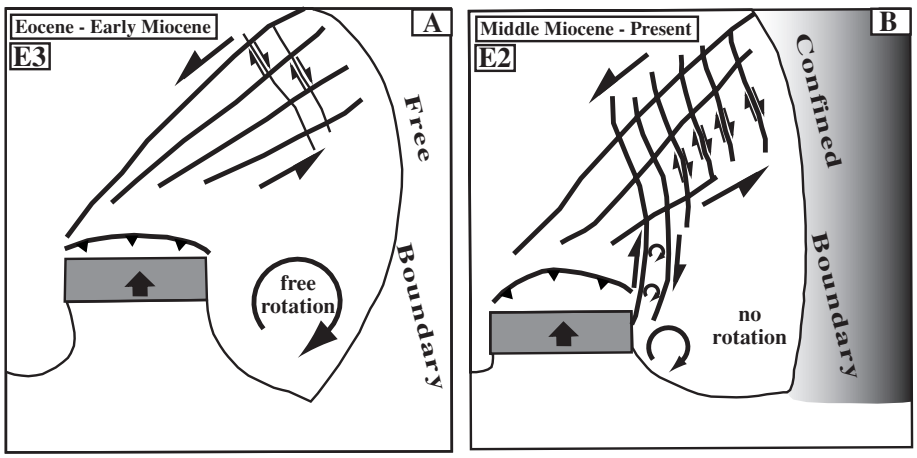


**Figure 11.** Schematic evolution of the large-scale deformation and rotations in southeastern Asia with respect to boundary conditions. During the first part of the collision (Eocene to Early Miocene), the eastern Asian boundary was free and southeast Asia rotated freely. During the second part of the collision (Middle Miocene to Present), the rotation of southeast Asia was precluded by the collisions of the Australian and Philippines Sea plates and the northward motion of Tibet relative to South China was taken up locally on the eastern margin of the Tibetan Plateau.

relative to South China to be taken up locally on the eastern margin of the Tibetan Plateau. This situation corresponds to the experiments E1 and E2 with an east-confined boundary: the southeastern part of the model is linked to the experimental box and the north–south right-lateral shear due to the northward motion of the indenter is taken up on the eastern edge of the indenter (Fig. 11b).

As suggested in Fig. 11, the change of boundary conditions in eastern Asia in Middle Miocene time with the collisions of the Australian and Philippines Sea plates, may have precluded the rotation of southeast Asia and provoked a large-scale change in the way in which the deformation is accommodated far from the subduction zones.

### 4.3 Opening of marginal basins

As stated in the first part, the geometry of backarc basins in eastern Asia is controlled by approximately north–south dextral strike-slip faults (Fournier 1994). In the Okhotsk Sea and North China Basins areas, the dextral Sakhalin–Hokkaido and Tanlu fault systems intersect with the conjugate and coeval sinistral Baikal–Stanovoy and Qinling fault systems, which pertain to the sinistral faults system extending from the Pamir zone to the Okhotsk Sea which accommodated the extrusion tectonics of Asia (Fig. 1a). The large-scale deformation pattern of Asia strongly suggests that the effects of the India–Eurasia collision extended at least as far northeastward as the Okhotsk Sea. The close similarity of the first-order deformation pattern of Asia to small-scale analogue models (Davy & Cobbold 1988) led Jolivet *et al.* (1990) to propose a model of opening of the northeast Asian basins (Japan sea and North China Basin) in relation to the India–Eurasia collision. In this model, the convergence between India and Asia is partly taken up along a wide left-lateral shear zone which connects the Pamir to the Stanovoy ranges and evolves from transpression to transtension (Fig. 1a). In the transtensional domain, left-lateral shear is accommodated by rotation of large crustal blocks bounded by right-lateral strike-slip zones, the east Japan Sea shear zone, the Tan-Lu Fault, and *en echelon* grabens on rims of the Ordos Block. Worrall *et al.* (1996) extended this model up to Kamchatka and the Bering Strait. Experiment E2 lends additional support to this interpretation, and even shows that left-lateral shear can be totally taken up by counter-clockwise rotations and right-lateral shear in the absence of major left-lateral shear zones.

In southeast Asia several backarc basins (South China Sea, Celebes and Sulu basins) opened during the Tertiary. It has been proposed that the opening of the South China Sea was related to the India–Eurasia collision (Tapponnier *et al.* 1982, 1986). In the experiments, no major shear zone interacts with the extensional domain to the southeast, which forms only as a consequence of gravitational spreading. According to the experiments, backarc basins in the north would thus be pull-apart basins controlled by dextral shear zones and basins in southeast Asia would be classical backarc basins with no interference with collision effects.

### 4.4 Asymmetric distribution of topography in Asia

The distribution of the topography in Asia is asymmetric with respect to the approximately north–south direction of the India–Asia convergence (Fig. 1b). Topography exceeds 1000 m throughout a triangular area heading northeast toward the Stanovoy ranges from the Himalayan arc. Higher topographies above 4000 m are found in Himalayas, Tibet and Pamir, i.e. in front of the Indian indenter, and along the northwestern margin of the topographic triangle which is marked by a series of mountain ranges including from southwest to northeast the Hindu Kush, the northern Pamir, the Tien Shan and the Altai. These mountain ranges belong to the Pamir–Baikal–Okhotsk left-lateral deformation zone. The same topographic distribution is observed in the experiments. A triangular thickened zone heading toward the northeast is observed in E4 (Fig. 8c) when the indentation velocity is several times higher than the spreading velocity. In E1 and E2 (Fig. 8c), a thickened zone is observed in the southwestern part of the major northeast-trending left-lateral shear zone.

## 5 CONCLUSION

We investigated the role of extension driven by gravity during continental deformation produced by collision, by means of analogue models. The experiments provide a model for the opening of the major marginal basins and continental grabens of eastern Asia related to right-lateral strike-slip faulting, in the framework of the India–Asia collision and the marginal extension above the retreating slabs of the western Pacific. Several origins have so far been proposed for the extensional deformation in Asia: subduction along the eastern and southeastern boundaries, collision with India and consecutive deformation of Asia, a mantle plume under the Baikal region and gravitational spreading in Tibet. In the case of subduction and a mantle plume, the high heat flow generated at the base of the crust would tend to decrease the integrated shear strength of the crust. This possibly makes it spread toward regions of low stress, e.g. subduction zones. If so, extension along subduction zones and above mantle plumes is driven by gravity, as in regions where the crust is thickened. We do not take into account thermal phenomena in the experiments. Gravity is used to produce extensional deformation along the boundaries of the model. As discussed above, this experimental assumption is not necessarily unrealistic. The experiments show that gravity and collision-related deformation interact in the northeastern part of the model, as continental deformation and subduction-related extension interacted in northeast Asia during the opening of the main basins. Because of the chosen rheology, the models do not show any rigid extrusion of a block that could be compared with Indochina. However, the experiments suggest that the opening of marginal basins in southeast Asia is more likely the result of subduction-related extension only.

Our experiments bring a physical basis to models which put the emphasis on a large-scale left-lateral shear zone running from the western Indian syntaxis to the Okhotsk Sea, to north–south-trending dextral shear zones which control the geometry of backarc basins, and to distributed extension in southeast Asia controlled solely by slab retreat. Whether extension is further enhanced by the thermal structure of the lithosphere (e.g. hot regions; Miyashiro 1986) is open to discussion.

## ACKNOWLEDGMENTS

The experiments were performed in the tectonic experimental laboratory at Rennes with the technical assistance of J. J. Kermarrec. We thank T. Nalpas and J.-M. Daniel for their help during the experiments and in computing the deformation grids, and Evgenii Burov and Hugues Raimbourg for scientific discussions during the review process. The manuscript greatly benefited from the reviews of Claudio Faccenna and Lucy Flesch. Figures were drafted using GMT software (Wessel & Smith 1991).

## REFERENCES


Achache, J., Courtillot, V. & Besse, J., 1983. Paleomagnetic constraints on the late Cretaceous and Cenozoic tectonics of southeastern Asia, *Earth planet. Sci. Lett.,* **63,** 123–136.

Allen, M.B., Macdonald, D.I.M., Vincent, S.J., Zhao, X. & Brouet-Menzies, C., 1997. Early Cenozoic two-phase extension and late Cenozoic thermal subsidence and inversion of the Bohai Basin, northern China, *Mar. Petrol. Geol.,* **14,** 951–972.

Arefiev, S., Rogozhin, E., Tatevossian, R., Rivera, L. & Cisternas, A., 2000. The Neftegorsk (Sakhalin Island) 1995 earthquake: a rare interplate event, *Geophys. J. Int.,* **143,** 595–608.

Argand, E., 1924. La tectonique de l'Asie, in *Congrès géologique International,* XIII Session, Belgique, pp. 171–372.

Argus, D.F. & Gordon, R.G., 1991. No-net-rotation model of current plate velocities incorporating plate motion model NUVEL-1, *Geophys. Res. Lett.,* **18,** 2039–2042.

Armijo, R., Tapponnier, P., Mercier, J.L. & Tonglin, H., 1986. Quaternary extension in southern Tibet: field observations and tectonic implications, *J. geophys. Res.,* **91,** 13 803–13 872.

Armijo, R., Tapponnier, P. & Tonglin, H., 1989. Late Cenozoic right-lateral strike-slip faulting in southern Tibet, *J. geophys. Res.,* **94,** 2787–2838.

Audley-Charles, M.G., 1981. Geometrical problems and implications of large scale overthrusting in the Banda Arc-Australian margin collision zone, in Thrust and Nappe Tectonics, *Geological Society of London Special Publication 9,* pp. 407–416, eds, McClay, K. & Price, N.J.

Avouac, J.P. & Tapponnier, P., 1993. Kinematic model of active deformation in central Asia, *Geophys. Res. Lett.,* **20,** 895–898.

Bellier, O., Mercier, J., Vergely, P., Long, C. & Ning, C., 1988. Evolution sédimentaire et tectonique du graben Mésozoique de la Wei He (province du Shanxi, Chine du Nord), *Bull. Soc. Geol. France,* **4,** 979–994.

Bird, P., 1991. Lateral extrusion of lower crust from under high topography in the isostatic limit, *J. geophys. Res.,* **96,** 10 275–10 286,

Briais, A., Patriat, P. & Tapponnier, P., 1993. Updated interpretation of magnetic anomalies and seafloor spreading stages in the South China Sea: implications for the tertiary tectonics of SE Asia, *J. geophys. Res.,* **98,** 6229–6328.

Burchfiel, B.C. & Royden, L.H., 1985. North-south extension within the convergent Himalayan region, *Geology,* **13,** 679–682.

Burchfiel, B.C. & Royden, L.H., 1991. Tectonics of Asia 50 years after the death of Emile Argand, *Eclogae Geol. Helv.,* **84,** 599–629.

Burchfiel, B.C., Zhiliang, C., Hodges, K.V., Yuping, L., Royden, L.H., Changrong, D. & Jiene, X., 1992. The south Tibetan detachment system, Himalayan orogen: extension comtemporaneous with and parallel to shortening in a collisional mountain belt, *Geol. Soc. Am. Spec. Pap.,* **269,** 1–41.

Burg, J.P., Guiraud, M., Chen, G.M. & Li, G.C., 1984. Himalayan metamorphism and deformations in the North Himalayan Belt (southern Tibet, China), *Earth planet. Sci. Lett.,* **69,** 391–400.

Byerlee, J.D., 1968. Brittle-ductile transition in rocks, *J. geophys. Res.,* **73,** 4741–4750,

Chamot-Rooke, N. & Pichon, X.L., 1989. Zenisu ridge: mechanical model of formation, *Tectonophysics,* **160,** 175–194.

Chamot-Rooke, N. & Le Pichon, X., 1999. GPS determined eastward Sundaland motion with respect to Eurasia confirmed by earthquakes slip vectors at Sunda and Philippine trenches, *Earth planet. Sci. Lett.,* **173,** 439–455.

Charlton, T.R., Barber, A.J. & Barkham, S.T., 1991. The structural evolution of the Timor collision complex, eastern Indonesia, *J. struct. Geol.,* **13,** 489–500.

Chen, W.P. & Nabelek, J., 1988. Seismogenic strike-slip faulting and the development of the North China basin, *Tectonics,* **7,**

Chen, Y., Courtillot, V., Cogné, J.P., Besse, J., Yang, Z. & Enkin, R.J., 1993. The configuration of Asia prior to the collision of India: Cretaceous paleomagnetic constraints, *J. geophys. Res.,* **98,** 21 927–21 941. 975–989.

Cobbold, P.R. & Davy, P., 1988. Indentation tectonics in nature and experiments. 2. Central Asia, *Bull. Geol. Inst. Upsalla,* **14,** 143–162.

Cohen, S.C. & Morgan, R.C., 1986. Intraplate deformation due to continental collisions: a numerical study of deformation in a thin viscous sheet, *Tectonophysics,* **132,** 247–259.

Coleman, M. & Hodges, K., 1995. Evidence for Tibetan Plateau uplift before 14 Myr ago from a new minimum age for east-west extension, *Nature,* **374,** 49–52.

Crétaux, J.-F., Soudarin, L., Cazenave, A. & Bouillé, F., 1998. Present-day tectonic plate motions and crustal deformations from the DORIS space system, *J. geophys. Res.,* **103,** 30 167–30 181.

Daly, M.C., Cooper, M.A., Wilson, I., Smith, D.G. & Hooper, B.G.D., 1991. Cenozoic plate tectonics and basin evolution in Indonesia, *Mar. Petrol. Geol.,* **8,** 2–21.

Davy, P. & Cobbold, P.R., 1988. Indentation tectonics in nature and experiments. Experiments scaled for gravity, *Bull. Geol. Inst. Upsalla,* **14,** 129–141.

Davy, P. & Cobbold, P.R., 1991. Experiments on shortening of a 4-layer model of the continental lithosphere, *Tectonophysics,* **188,** 1–25.

Davy, P., Hansen, A., Bonnet, E. & Zhang, S.-Z., 1995. Localization and fault growth in layered brittle-ductile systems: Implications for deformations of the continental lithosphere, *J. geophys. Res.,* **100,** 6281–6294.

DeMets, C., Gordon, R.G., Argus, D.F. & Stein, S., 1990. Current plate motion, *Geophys. J. Int.,* **101,** 425–478.

DeMets, C., Gordon, R.G., Argus, D.F. & Stein, S., 1994. Effects of recent revisions to the geomagnetic reversal time scale on estimates of current plates motions, *Geophys. Res. Lett.,* **21,** 2191–2194.

Deverchère, J., Houdry, F., Solonenko, N.V., Solonenko, A.V. & Sankov, V.A., 1993. Seismicity, active faults and stress field of the north Muya region, Baikal rift: new insights on the rheology of extended continental lithosphere, *J. geophys. Res.,* **98,** 19 895–19 912.

Dewey, J.F., Shackleton, R.M., Chang Chengfa, Chang Chengfa & Sun Yiyin, 1988. The tectonic evolution of the Tibetan plateau, *Phil. Trans. R. Soc. Lond.,* A, **327,** 379–413,

Dewey, J.F., Cande, S. & Pitman, W.C.I., 1989. Tectonic evolution of the India-Eurasia collision zone, *Eclogae geol. Helv.,* **82,** 717–734.

Eguchi, T. & Uyeda, S., 1983. Seismotectonics of the Okinawa trough and Ryukyu arc, *Mem. Geol. Soc. China.,* **5,** 189–210.

Engdahl, E.R., van der Hilst, R. & Buland, R., 1998. Global teleseismic earthquake relocation with improved travel times and procedures for depth determination, *Bull. seism. Soc. Am.,* **88,** 722–743.

England, P. & Houseman, G.A., 1986. Finite strain calculations of continental deformation. II: application to the India-Asia collision, *J. geophys. Res.,* **91,** 3664–3676.

England, P. & McKenzie, D.P., 1982. A thin viscous sheet model for continental deformation, *Geophys. J. R. astr. Soc.,* **70,** 295–321.

England, P. & Molnar, P., 1990. Right-lateral shear and rotation as the explanation for strike-slip faulting in eastern Tibet, *Nature,* **344,** 140–142.

England, P. & Molnar, P., 1997. The field of crustal velocity in Asia calculated from Quaternary rates of slip on faults, *Geophys. J. Int.,* **130,** 551–582.

England, P., Houseman, G.A. & Sonder, L., 1985. Length scales for continental deformation in convergent, divergent, and strike-slip environments: Analytical and approximate solutions for a thin viscous sheet model, *J. geophys. Res.,* **90,** 523–532.

Faccenna, C., Davy, P., Brun, J.P., Funiciello, R., Giardini, D., Mattei, M. & Nalpas, T., 1996. The dynamics of back-arc extensions: a laboratory approach to the opening of the Tyrrhenian Sea, *Geophys. J. Int.,* **126,** 781–795.

Faccenna, C., Giardini, D., Davy, P. & Argentieri, A., 1999. Initiation of subduction at Atlantic-type margins: insights from laboratory experiments, *J. geophys. Res.,* **104,** 2749–2766.

Flesch, L.M., Haines, A.J. & Holt, W.E., 2001. Dynamics of the India-Eurasia collision zone, *J. geophys. Res.,* **106,** 16 435–16 460.

Fournier, M., 1994. Ouverture de bassins marginaux et déformation continentale: l'exemple de la mer du Japon, *PhD thesis,* Université de Paris 6, p. 312.

Fournier, M., Jolivet, L., Huchon, P., Rozhdestvensky, V.S., Sergeyev, K.F. & Oscorbin, L., 1994. Neogene strike-slip faulting in Sakhalin, and the Japan Sea opening, *J. geophys. Res.,* **99,** 2701–2725.

Fournier, M., Jolivet, L. & Fabbri, O., 1995. Neogene stress field in SW Japan and mechanism of deformation during the Japan Sea opening, *J. geophys. Res.,* **100,** 24 295–24 314.

Fournier, M., Fabbri, O., Angelier, J. & Cadet, J.P., 2001. Kinematics and timing of opening of the Okinawa Trough: insights from regional seismicity and onland deformation in the Ryukyu arc, *J. geophys. Res.,* **106,** 13 751–13 768.

Fukao, Y. & Furumoto, M., 1975. Mechanisms of large earthquakes along the eastern margin of the Japan Sea, *Tectonophysics,* **25,** 247–266.

Funahara, S., Nishiwaki, N., Miki, M., Muruta, F., Otofuji, Y. & Yi Zhao Wang, 1992. Paleomagnetic study of Cretaceous rocks from the Yangtze block, central Yunnan, China: implications for the India-Asia collision, *Earth planet. Sci. Lett.,* **113,** 77–91.

Funahara, S., Nishiwaki, N., Muruta, F., Otofuji, Y. & Yi Zhao Wang, 1993. Clockwise rotation of the Red River fault inferred from paleomagnetic study of Cretaceous rocks in the Shan-Thai-Malay block of western Yunnan, China, *Earth planet. Sci. Lett.,* **117,** 29–42.

Halim, N. *et al.*, 1998. New Cretaceous and Early Tertiary paleomagnetic results from Xining-Lanzhou basin, Kunlun and Qiangtang blocks, China: Implications on the geodynamic evolution of Asia, *J. geophys. Res.,* **103,** 21 025–21 045.

Hall, R., 1996. Reconstructing Cenozoic SE Asia, in *Tectonic Evolution of Southeast Asia,* Geological Society of London Special Publication 106, pp. 153–184, eds Hall, R. & Blundell, D.

Hall, R., 2002. Cenozoic geological and plate tectonic evolution of SE Asia and the SW Pacific: computer-based reconstructions, model and animations, *J. Asian Earth Sci.,* **20,** 353–431.

Hamilton, W., 1979. *Tectonics of the Indonesian Region,* US Geological Survey Professional Paper 1078, p. 345.

Harris, R.A., 1991. Temporal distribution of strain in the active Banda orogen: a reconciliation of rival hypotheses, in *Orogeneis in Action, Journal of Asian Earth Science Special Issue 5,* **6,**(3/4), pp. 373–386, eds Hall, R., Nichols, G. & Rangin, C.

Harrison, T.M., Leloup, P.H., Ryerson, F.J., Tapponnier, P., Lacassin, R. & Chen, W., 1996. Diachronous initiation of transtension along the Ailao San-Red River shear zone, Yunnan and Vietnam, in *The Tectonic Evolution of Asia,* pp. 208–226, eds Lin, A. & Harrison, T.M., Cambridge University Press, New York.

Heki, K., 1996. Horizontal and vertical crustal movements from three-dimensional very long baseline interferometry kinematic reference frame: implication for the reversal timescale revision, *J. geophys. Res.,* **101,** 3187–3198.

Heki, K., Takahashi, Y. & Kondo, T., 1990. Contraction of northeastern Japan: evidence from horizontal displacement of a Japanese station in global very long baseline interferometry networks, *Tectonophysics,* **181,** 113–122.

Heki, K. *et al.*, 1999. The Amurian Plate motion and current plate kinematics in eastern Asia, *J. geophys. Res.,* **104,** 29 147–29 155.

Hellinger, S.J., Shedloock, K.M., Sclater, J.G. & Hong, Y., 1985. The Cenozoic evolution of the noth China basin, *Tectonics,* **4,** 343–358.

Henry, P., Mazzotti, S. & Le Pichon, X., 2001. Transient and permanent deformation of central Japan estimated by GPS—1. Interseismic loading and subduction kinematics, *Earth planet. Sci. Lett.,* **184,** 443–453.

Ho, C.S., 1986. A synthesis of the geological evolution of Taiwan, *Tectonophysics,* **125,** 1–16.

Holloway, N.H., 1982. The stratigraphy and tectonic relationship of Reed Bank, north Palawan and Mindoro to the Asian mainland and its significance in the evolution of the South China Sea, *Am. Assoc. Petrol. Bull.,* **66,** 1357–1383.

Holt, E.H. & Haines, A.J., 1993. Velocity field in deforming Asia from the inversion of earthquake-released strains, *Tectonics,* **12,** 1–20.

Holt, E.H., Ni, J.F., Wallace, T.C. & Haines, A.J., 1991. The active tectonics of the eastern Himalayan syntaxis and surrounding regions, *J. geophys. Res.,* **96,** 14 595–14 632.

Holt, E.H., Li, M. & Haines, A.J., 1995. Earthquake strain rates and instantaneous relative motion within central and east Asia, *Geophys. J. Int.,* **122,** 569–593.

Holt, W.E., Chamot-Rooke, N., Le Pichon, X., Haines, A.J., Shen-Tu, B. & J. Ren, 2000. Velocity field in Asia inferred from Quaternary fault slip rates and Global Positioning System observations, *J. geophys. Res.,* **105,** 19 185–19 209.

Hong, Y., Shedlock, K.M., Hellinger, S.J. & Sclater, J.G., 1985. The North China Basin: an example of a Cenozoic rifted intraplate basin, *Tectonics,* **4,** 153–169.

Houseman, G. & England, P., 1986. Finite strain calculations of continental deformation. 1. Method and general results for convergent zones, *J. geophys. Res.,* **91,** 3651–3663.

Houseman, G. & England, P., 1993. Crustal thickening versus lateral expulsion in the Indian-Asian continental collision, *J. geophys. Res.,* **98,** 12 233–12 249.

Houseman, G. & England, P., 1996. A lithospheric-thickening model for the Indo-Asian collision, in *Tectonic Evolution of Asia,* pp. 3–17, eds Yin, A. & Harrison, T.M., Cambridge University Press, New York.

Huang, K. & Opdyke, N.D., 1993. Paleomagnetic results from Cretaceous and Jurassic rocks of south and southwest Yunnan: evidence for large clockwise rotations in the Indochina and Shan-Thai-Malay terranes, *Earth planet. Sci. Lett.,* **117,** 507–524.

Huang, K., Opdyke, N.D., Li, J. & Peng, X., 1992. Paleomagnetism of Cretaceous rocks from eastern Qiangtang terrane of eastern Tibet, *J. geophys. Res.,* **97,** 1789–1799.

Hutchinson, D.R., Golmshtok, A.J., Zonenshain, L.P., Moore, T.C., Scholz, C.A. & Klitgord, K.D., 1992. Depositional and tectonic framework of the rift basins of Lake Baikal from multichannel seismic data, *Geology,* **20,** 589–592.

Imanishi, M., Kimata, F., Inamori, N., Miyajima, R., Okuda, T., Takai, K., Hirahara, K. & Kato, T., 1996. Horizontal displacements by GPS measurements at the Okinawa-Sakishima Islands (1994–1995), *J. Seismol. Soc. Japan,* **49,** 417–421.

Itoh, Y., 1988. Differential rotation of the eastern part of Southwest Japan inferred from paleomagnetism of Cretaceous and Neogene rocks, *J. geophys. Res.,* **93,** 3401–3411.

Jaeger, J.C. & Cook, N.G.W., 1979. *Fundamentals of Rock Mechanics,* 3rd edn, Chapman and Hall, London.

Jolivet, L. & Huchon, P., 1989. Crustal scale strike-slip deformation in Hokkaido, Northeast Japan, *J. struct. Geol.,* **11,** 509–522.

Jolivet, L. & Tamaki, K., 1992. Neogene kinematics in the Japan Sea region and the volcanic activity of the Northeast Japan arc, in *Proc. ODP, Sci. Results,* pp. 1311–1331, eds Tamaki, K., Suyehiro, K., Allan, J., McWilliams, M., Ocean Drilling Program, College Station, TX.

Jolivet, L., Davy, P. & Cobbold, P., 1990. Right-lateral shear along the northwest Pacific margin and the India-Eurasia collision, *Tectonics,* **9,** 1409–1419.

Jolivet, L., Huchon, P., Brun, J.P., Chamot-Rooke, N., Le Pichon, X. & Thomas, J.C., 1991. Arc deformation and marginal basin opening, Japan Sea as a case study, *J. geophys. Res.,* **96,** 4367–4384.

Jolivet, L., Fournier, M., Huchon, P., Rozhdestvenskiy, V.S., Sergeyev, S. & Oscorbin, L.S., 1992. Cenozoic intracontinental dextral motion in the Okhotsk-Japan Sea region, *Tectonics,* **11,** 968–977.

Jolivet, L., Tamaki, K. & Fournier, M., 1994. Japan Sea, opening history and mechanism, a synthesis, *J. geophys. Res.,* **99,** 22 237–22 259.

Jolivet, L., Lepvrier, C., Maluski, H., Beyssac, O., Goffé, B., Nguyen Van Vuong, Nguyen Van Vuong & Phan Truong Thi, 1999. Oligocene-Miocene Bu Khang extensional gneiss dome in Vietnam: geodynamic implications, *Geology,* **27,** 67–70.

Karig, D.E., 1971. Origin and development of marginal basins in the western Pacific, *J. geophys. Res.,* **76,** 2542–2561.

Kimura, G. & Tamaki, K., 1986. Collision, rotation and back arc spreading: the case of the Okhotsk and Japan seas, *Tectonics,* **5,** 389–401.

Kong, X. & Bird, P., 1996. Neotectonics of Asia: thin-shell finite-element models with faults, in *Tectonic Evolution of Asia,* pp. 18–34, eds Yin, A. & Harrison, T.M., Cambridge University Press, New York.

Lallemand, S. & Jolivet, L., 1985. Japan Sea: a pull apart basin, *Earth planet. Sci. Lett.,* **76,** 375–389.

Lallemant, S., Chamot-Rooke, N., Le Pichon, X. & Rangin, C., 1989. Zenisu Ridge: a deep intra-oceanic thrust related to subduction off southwest Japan, *Tectonophysics,* **160,** 151–174.

Larson, K.M., Bürgmann, R., Bilham, R. & Freymueller, J.T., 1999. Kinematics of the India-Eurasia collision zone from GPS measurements, *J. geophys. Res.,* **104,** 1077–1093.

Leloup, P.H. *et al.,* 1995. The Ailao Shan-Red River shear zone (Yunnan, China), Tertiary transform boundary of Indochina, *Tectonophysics,* **251,** 3–84.

Leloup, P.H., Arnaud, N., Lacassin, R., Kienast, J.R., Harrison, T.M., Phan Trong, T.T., Replumaz, A. & Tapponnier, P., 2001. New constraints on the structure, thermochronology, and timing of the Ailao Shan-Red River shear zone, SE Asia, *J. geophys. Res.,* **106,** 6683–6732.

Le Pichon, X., 1982. Land-locked ocean basin and continental collision in the eastern Mediterranean area as a case example, in *Mountain Building Process,* pp. 201–213, ed. Hsu, K.J., Academic, San Diego, CA.

Le Pichon, X., Fournier, M. & Jolivet, L., 1992. Kinematics, topography, shortening and extrusion in the India-Eurasia collision, *Tectonics,* **11,** 1085–1098.

Lu, H., Yu, H., Ding, Y. & Zhang, Q., 1983. Changing stress field in the middle segment of the Tan-Lu fault zone, eastern China, *Tectonophysics,* **98,** 253–270.

Ma, X. & Wu, D., 1987. Cenozoic extensional tectonics in China, *Tectonophysics,* **133,** 243–255.

Maleterre, P., 1989. Histoire sédimentaire, magmatique, tectonique et métallogénique d'un arc cénozoique déformé en régime de transpression, *Thèse de doctorat,* p. 304, Université Bretagne Occidentale.

Marquis, G., Roques, D., Huchon, P., Coulon, O., Chamot-Rooke, N., Rangin, C. & Le Pichon, X., 1997. Amount and timing of extension along the continental margin off central Vietnam, *Bull. Soc. Géol. France,* **168,** 707–716.

Martinod, J. & Davy, P., 1994. Periodic instabilities during compression of the lithosphere, 2, Analogue experiments, *J. geophys. Res.,* **99,** 12 057–12 069.

Mazzotti, S., Henry, P., Le Pichon, X. & Sagiya, T., 1999. Strain partitioning in the zone of transition from Nankai subduction to Izu-Bonin collision (Central Japan): implications for an extensional tear within the subducting slab, *Earth planet. Sci. Lett.,* **172,** 1–10.

Mazzotti, S., Henry, P. & Le Pichon, X., 2001. Transient and permanent deformation of central Japan estimated by GPS—2. Strain partitioning and arc-arc collision, *Earth planet. Sci. Lett.,* **184,** 455–469.

McKenzie, D.P., 1969. Speculations on the consequences and causes of plate motions, *Geophys. J. R. astr. Soc.,* **18,** 1–32,

McKenzie, D.P. & Jackson, J., 1983. The relationship between strain rates, crustal thickening, paleomagnetism, finite strain and fault movements within a deforming zone, *Earth planet. Sci. Lett.,* **65,** 182–202.

Mercier, J.L., Armijo, R., Tapponnier, P., Carey-Gailhardis and Lin, H.T., 1987. Change from Late Tertiary compression to Quaternary extension in southern Tibet during the India-Asia collision, *Tectonics,* **6,** 275–304.

Milsom, J. & Audley-Charles, M.R., 1986. Post collisional isostatic adjustment in the southern Banda arc, in *Collision Tectonics,* Geological Society of London Special Publication, eds Coward M.P. & Ries, A.C. pp. 353–366.

Miyashiro, A., 1986. Hot regions and the origin of marginal basins in the western Pacific, *Tectonophysics,* **122,** 195–216.

Molnar, P. & Atwater, T., 1978. Interarc spreading and cordilleran tectonics as alternates related to the age of the subducted oceanic lithosphere, *Earth planet. Sci. Lett.,* **41,** 330–340.

Molnar, P. & Chen, W.P., 1983. Focal depths and fault plane solutions of earthquakes under the Tibetan plateau, *J. geophys. Res.,* **88,** 1180–1196.

Molnar, P. & Deng Q., 1984. Faulting associated with large earthquakes and the average rate of deformation in central and eastern Asia, *J. geophys. Res.,* **89,** 6203–6227.

Molnar, P. & Gipson, J.M., 1996. A bound on the rheology of continental lithosphere using very long baseline interferometry: the velocity of south China with respect to Eurasia, *J. geophys. Res.,* **101,** 545–554.

Molnar, P. & Lyon-Caen, H., 1989. Fault plane solutions of earthquakes and active tectonics of the Tibetan plateau and its margins, *Geophys. J. Int.,* **99,** 123–153.

Molnar, P. & Tapponnier, P., 1975. Cenozoic tectonics of Asia: effects of a continental collision, *Science,* **189,** 419–426.

Molnar, P. & Tapponnier, P., 1978. Active tectonics of Tibet, *J. geophys. Res.,* **83,** 5361–5375.

Molnar, P., Burchfield, B.C., K'uangyi, L. & Ziyun, Z., 1987. Geomorphic evidence for active faulting in the Altyn Tagh and northern Tibet and qualitative estimates of its contribution to the convergence of India and Eurasia, *Geology,* **15,** 249–253.

Nabelek, J., Chen, W.P. & Ye, H., 1987. The Tangshan earthquake sequence of 1976 and its implications for the evolution of the North China basin, *J. geophys. Res.,* **92,** 12 615–12 628.

Nakamura, K. & Uyeda, S., 1980. Stress gradient in back arc regions and plate subduction, *J. geophys. Res.,* **85,** 6419–6428.

Otofuji, Y., Inoue, Y., Funahara, S., Murata, F. & Zheng, X., 1990. Paleomagnetic study of eastern Tibet—deformation of the Three Rivers region, *Geophys. J. Int.,* **103,** 85–94.

Pan, Y. & Kidd, W.S.F., 1992. Nyainqentanghla shear zone: a late Miocene extensional detachment in the southern Tibetan plateau, *Geology,* **20,** 775–778.

Parfenoy, L.M., Kozmin, B.M., Imayev, V.S. & Savostin, L.A., 1987. The tectonic character of the Olekma–Stanovoy Seismic zone, *Geotectonics,* **21,** 560–572.

Peltzer, G. & Saucier, F., 1996. Present-day kinematics of Asia derived from geological fault rates, *J. geophys. Res.,* **101,** 27 943–27 956.

Peltzer, G. & Tapponnier, P., 1988. Formation and evolution of strike-slip faults, rifts and basins during the India-Asia collision: an experimental approach, *J. geophys. Res.,* **93,** 15 085–15 118.

Qin, C., Papazachos, C. & Papadimitriou, E., 2002. Velocity field for crustal deformation in China derived from seismic moment tensor summation of earthquakes, *Tectonophysics,* **359,** 29–46.

Ramsay, J.G., 1967. *Folding and Fracturing of Rocks,* p. 560, McGraw-Hill, New York.

Ranalli, G., 1995. *Rheology of the Earth,* Chapman and Hall, New York.

Rangin, C., Jolivet, L., Pubellier, M. *et al.*, 1990. A simple model for the tectonic evolution of southeast Asia and Indonesia region for the past 43 Ma, *Bull. Soc. Géol. France,* **6,** 889–906.

Ren, J., Tamaki, K., Sitian, Li & Zhang Junxia, 2002. Late Mesozoic and Cenozoic rifting and its dynamic setting in Eastern China and adjacent areas, *Tectonophysics,* **344,** 175–205.

Replumaz, A., 1999. Reconstruction de la zone de collision Inde-Asie: etude centrée sur l'Indochine, *PhD thesis*, p. 229, Université Paris 7, Paris.

Roques, D., Rangin, C. & Huchon, P., 1997. Geometry and sense of motion along the Vietnam continental margin: onshore/offshore Da Nang area, *Bull. Soc. Géol. France,* **168,** 413–422.

Salençon, J., 1995. *Mécanique du Continu, Tome 1, Concepts Généraux,* p. 352, Ellipse, Paris.

Shemenda, A.I. & Grokholski, A.L., 1992. Physical modelling of lithosphere in collision zones, *Tectonophysics,* **216,** 273–290.

Shen, Z.-K., Zhao, C., Yin, A., Li, Y., Jackson, D.D., Fang, P. & Dong, D., 2000. Contemporary crustal deformation in east Asia constrained by Global Positioning System measurements, *J. geophys. Res.,* **105,** 5721–5734.

Sibuet, J.C. *et al.*, 1987. Back-arc extension in the Okinawa trough, *J. geophys. Res.,* **92,** 14 041–14 063.

Sibuet, J.C., Hsu, S.-K., Shyu, C.T. & Liu, C.S., 1995. Structural and kinematic evolutions of the Okinawa Trough backarc basin, in *Backarc Basins: Tectonics and Magmatism,* pp. 343–379, ed. Taylor, B., Plenum, New York.

Sibuet, J.C., Deffontaines, B., Hsu, S.-K., Thareau, N., Le Formal, J.P., Liu, C.S. & the ACT Party, 1998. Okinawa trough backarc basin: early tectonic and magmatic evolution, *J. geophys. Res.,* **103,** 30 245–30 267.

Silver, E.A. & Rangin, C., 1991a. Developement of the Celebes Sea basin in the context of Western Pacific marginal basins history, in *Proc. ODP, Sci. Results,* pp. 39–50, eds Silver, E.A., Rangin, C., Breymann, M.T. & Fisk, M., Ocean Drilling Program, College Station, TX.

Silver, E.A. & Rangin, C., 1991b. Leg 124 tectonic synthesis, in *Proc. ODP, Sci. Results,* pp. 3–10, eds Silver, E.A., Rangin, C., Breymann, M. T. & Fisk, M., Ocean Drilling Program, College Station, TX.

Silver, E.A., McCaffrey, R. & Smith, R.B., 1983a. Collision, rotation, and the initiation of subduction in the evolution of the Sulawesi, Indonesia, *J. geophys. Res.,* **88,** 9407–9418.

Silver, E.A., Reed, D., McCaffrey, R. & Joyodiwiryo, Y., 1983b. Back arc thrusting in the eastern Sunda arc, Indonesia: a consequence of arc-continent collision, *J. geophys. Res.,* **88,** 7429–7448.

Tamaki, K., 1988. Geological structure of the Japan sea and its tectonic implications, *Bull. geol. Surv. Japan,* **39,** 269–365.

Tamaki, K., Suyehiro, K., Allan, J., Ingle, J.C. & Pisciotto, K., 1992. Tectonic synthesis and implications of Japan Sea ODP drilling, in *Proc. ODP, Sci. Results,* pp. 1333–1350, eds, Tamaki, K., Suyehiro, K., Allan, J. & McWilliams, M., Ocean Drilling Program, College Station, TX.

Tapponnier, P. & Molnar, P., 1976. Slip line field theory and large-scale continental tectonics, *Geology,* **264,** 319–324.

Tapponnier, P. & Molnar, P., 1979. Active faulting and Cenozoic tectonic of the Tien Shan, Mongolia, and Baykal regions, *J. geophys. Res.,* **84,** 3425–3459.

Tapponnier, P., Mercier, J.L., Armijo, R., Han, T. & Zhou, J., 1981. Field evidences for active normal faulting in Tibet, *Geology,* **294,** 410–414.

Tapponnier, P., Peltzer, G., Dain, A.Y.L., Armijo, R. & Cobbold, P., 1982. Propagating extrusion tectonics in Asia: new insights from simple experiments with plasticine, *Geology,* **10,** 611–616.

Tapponnier, P., Peltzer, G. & Armijo, R., 1986. On the mechanics of the collision between India and Asia, in *Collision Tectonics,* Geological Society of London Special Publication, pp. 115–157, eds Coward M.P. & Ries, A.C.

Tatsumi, Y., Otofuji, Y.I., Matsuda, T. & Nohda, S., 1989. Opening of the Sea of Japan back-arc basin by asthenospheric injection, *Tectonophysics,* **166,** 317–329.

Taylor, B. & Hayes, D.E., 1980. The tectonic evolution of the south China basin, in *The Tectonic and Geological Evolution of Southeast Asian Seas and Islands,* pp. 89–104, ed. Hayes, D.E., American Geophysical Union, Washington, DC.

Thomas, J.C., Lanza, R., Kazansky, A., Zykin, V., Semakov, N., Mitrokhin, D. & Delvaux, D., 2002. Paleomagnetic study of Cenozoic sediments from the Zaisan basin (SE Kazakhstan) and the Chuya depression (Siberian Altai): tectonic implications for central Asia, *Tectonophysics,* **351,** 119–137.

Tian, Z., Hang, P. & Xu, K.D., 1992. The Mesozoic-Cenozoic east China rift system, *Tectonophysics,* **208,** 341–363.

Uyeda, S. & Kanamori, H., 1979. Backarc opening and the mode of subduction, *J. geophys. Res.,* **84,** 1049–106.

Vilotte, J.P., Daignières, M. & Madariaga, R., 1982. Numerical modeling of intraplate deformation: simple mechanical models of continental collision, *J. geophys. Res.,* **87,** 10 709–10 728.

Vilotte, J.P., Daignieres, M., Madariaga, R. & Zienkiewicz, O.C., 1984. The role of a heterogeneous inclusion during continental collision, *Phys. Earth planet. Int.,* **36,** 236–259.

Vilotte, J.P., Madariaga, R., Daignieres, M. & Zienkiewicz, O.C., 1986. Numerical study of continental collision: influence of buoyancy forces and an initial stiff inclusion, *Geophys. J. R. astr. Soc.,* **84,** 279–310.

Wang, J.M., 1987. The Fenwei rift and its recent periodic activity, *Tectonophysics,* **133,** 257–275.

Wang, Q. et al, 2001. Present-day crustal deformation in China constrained by global positioning system measurements, *Science,* **294,** 574–577.

Weissel, J.K., 1980. Evidence for Eocene oceanic crust in the Celebes basin, in *The Tectonic and Geological Evolution of Southeast Asian Seas and Islands,* pp. 37–47, ed. Hayes, D.E., American Geophysical Union, Washington, DC.

Wessel, P. & Smith, W.M.F., 1991. Free software helps map and display data, *EOS, Trans. Am. geophys. Un.,* **72,** 441–446.

Windley, B.F. & Allen, M.B., 1993. Mongolian plateau: evidence for a late Cenozoic mantle plume under central Asia, *Geology,* **21,** 295–298.

Worrall, D.M., Kruglyak, V., Kunst, F. & Kusnetsov, V., 1996. Tertiary tectonics of the Sea of Okhotsk, Russia: far-field effects of the India-Asia collision, *Tectonics,* **15,** 813–826.

Xu, J., Zhu, G., Tong, W.X., Cui, K.R. & Liu, Q., 1987. Formation and evolution of the Tancheng–Lujiang wrench fault system to the northwest of the Pacific ocean, *Tectonophysics,* **134,** 273–310.

Xu, X. & Ma, X., 1992. Geodynamics of the Shanxi rift system, *Tectonophysics,* **208,** 325–340.

Yamagishi, H. & Watanabe, Y., 1986. Change of stress field in Late Cenozoic, Southwest Hokkaido, Japan—investigation of geological faults, dykes, ore veins and active faults, *Monograph Geol. Collabor. Jpn.,* **31,** 321–332.

Yamazaki, K., Tamura, T. & Kawasaki, I., 1985. Seismogenic stress field of the Japan Sea as derived from shallow and small earthquakes, *J. seism. Soc. Japan,* **38,** 541–558.

Yu, S.B. & Chen, H.Y., 1994. Global positioning system measurements of crustal deformation in the Taiwan arc-continent collision zone, *Mem. Geol. Soc. China,* **5,** 477–498.